Published in final edited form as:
J Neurosci. 2012 October 17; 32(42): 14775–14793. doi:10.1523/JNEUROSCI.2060-12.2012.

Oligodendrocyte Regeneration after Neonatal Hypoxia Requires FoxO1-Mediated p27^{Kip1} Expression

Beata Jablonska[1], **Joseph Scafidi**[1], **Adan Aguirre**[2], **Flora Vaccarino**[3,4], **Vien Nguyen**[6], **Erzsebet Borok**[4,5], **Tamas L. Horvath**[4,5], **David H. Rowitch**[6], and **Vittorio Gallo**[1]

[1]Center for Neuroscience Research, Children's National Medical Center, Washington, DC 20010-2970

[2]Pharmacological Sciences, Stony Brook University, Stony Brook, New York 11794-5140

[3]Child Study Center, Yale University, New Haven, Connecticut 06520

[4]Department of Neurobiology, Yale University, New Haven, Connecticut 06520

[5]Department of Obstetrics, Gynecology, and Reproductive Sciences, Yale University, New Haven, Connecticut 06520

[6]Departments of Pediatrics and Neurosurgery, Eli and Edythe Broad Institute for Stem Cell Research and Regeneration Medicine and Howard Hughes Medical Institute, University of California, San Francisco, San Francisco, California 94143

Abstract

Diffuse white matter injury (DWMI) caused by hypoxia is associated with permanent neurodevelopmental disabilities in preterm infants. The cellular and molecular mechanisms producing DWMI are poorly defined. Using a mouse model of neonatal hypoxia, we demonstrate a biphasic effect on oligodendrocyte development, resulting in hypomyelination. Oligodendrocyte death and oligodendrocyte progenitor cell (OPC) proliferation during the week after hypoxia were followed by delayed oligodendrocyte differentiation and abnormal myelination, as demonstrated by electron microscopy. Cdk2 activation was essential for the regenerative OPC response after hypoxia and was accompanied by reduced FoxO1-dependent p27 ^{Kip1} expression. p27 ^{Kip1} was also reduced in OPCs in human infant white matter lesions after hypoxia. The negative effects of hypoxia on oligodendrogenesis and myelination were more pronounced in p27 ^{Kip1}-null mice; conversely, overexpression of FoxO1 or p27 ^{Kip1} in OPCs after hypoxia promoted oligodendrogenesis. Our studies demonstrate for the first time that neonatal hypoxia affects the Foxo1/p27 ^{Kip1} pathway during white matter development. We also show that molecular manipulation of this pathway enhances oligodendrocyte regeneration during a critical developmental time window after DWMI. Thus, FoxO1 and p27 ^{Kip1} may serve as promising target molecules for promoting timely oligodendrogenesis in neonatal DWMI.

Correspondence should be addressed to Dr. Vittorio Gallo, Center for Neuroscience Research, Children's National Medical Center, 111 Michigan Avenue, Northwest, Washington, DC 20010. vgallo@cnmcresearch.org.

Author contributions: B.J., J.S., A.A., and V.G. designed research; B.J., J.S., A.A., V.N., E.B., T.L.H., and D.H.R. performed research; F.V. contributed unpublished reagents/analytic tools; B.J. and V.N. analyzed data; B.J., V.N., D.H.R., and V.G. wrote the paper.

The authors declare no competing financial interests.

Introduction

Chronic neurological disabilities—including motor, cognitive, and behavioral delays—occur with increased frequency in premature infants of very low birth weight, as do behavioral disorders, epilepsy, and cerebral palsy (Hack et al., 2000; Wood et al., 2000; Volpe, 2001). These infants are at high risk of developing diffuse white matter injury (DWMI) previously referred to as periventricular leukomalacia (Back, 2006). Premature infants with evidence of DWMI on MRI at term equivalent age (Ment et al., 1998, 2000) and those with severe respiratory problems (e.g., bronchopulmonary dysplasia) and recurrent hypoxemia are at high risk for long-term neurological deficits (Ment et al., 2003; Fagel et al., 2009; Scafidi et al., 2009). Morphological and structural changes in the brain—with main disturbances occurring in the white matter—lead to chronic disability in survivors (Ment et al., 1998, 2000). The alterations in white matter development due to neonatal brain damage are usually associated with significant disruption of myelination (Kinney and Back, 1998), which correlates with a period of developmentally regulated susceptibility of late oligodendrocyte progenitor cells (OPCs) (Back et al., 2002). Therefore, identification of molecular mediators of oligodendrocyte regeneration in neonatal white matter following hypoxia *in vivo* is essential for developing therapeutic strategies to prevent neurodevelopmental deficits associated with this pathology in premature infants.

Oligodendrocyte regeneration in adult white matter under pathological conditions involves recruitment of local (parenchymal) and remote [subventricular zone (SVZ)]-derived OPCs (Aguirre et al., 2007). The SVZ, a major germinal area in humans and rodents (Luskin, 1993; Lachapelle et al., 2002; Sanai et al., 2004; Menn et al., 2006; Jablonska et al., 2007; Nait-Oumesmar et al., 2008), contains a substantial pool of OPCs, which—under pathological conditions—can generate new oligodendrocytes in affected white matter regions (Armstrong et al., 2002; Frost et al., 2003; Crockett et al., 2005; Aguirre et al., 2007). However, the cellular responses induced by neonatal hypoxia in white matter and SVZ OPCs, and the molecular pathways regulating oligodendrocyte regeneration from these cells *in vivo*, are still undefined.

The present study used a clinically relevant mouse model of DWMI (Fagel et al., 2009; Scafidi et al., 2009; Bi et al., 2011) to investigate the impact of this injury on oligodendrocyte and white matter development. We analyzed the response of endogenous OPCs to DWMI, with the goal of identifying specific signaling pathways that could be targeted to enhance cellular recovery. We found that neonatal hypoxia caused abnormalities in developmental myelination due to apoptosis and delayed maturation of oligodendrocytes during a critical developmental time window. Furthermore, hypoxia activated the Cdk2 signaling pathway in white matter OPCs to induce proliferation of these cells, while expressions of p27 ^{Kip1} and of its regulator FoxO1 were significantly reduced. Decreased p27 ^{Kip1} expression was also found in OPCs in white matter lesions of human newborns with neonatal hypoxic brain damage. The effects of DWMI on oligodendrocyte development were more pronounced in p27 ^{Kip1}-null mice, while overexpression of FoxO1 or p27 ^{Kip1} promoted oligodendrocyte differentiation and was protective. Thus the FoxO1–p27 ^{Kip1} pathway was identified as a crucial regulator of OPC differentiation after neonatal hypoxia.

Materials and Methods

Animals and hypoxic treatment

Colonies of CNP-EGFP (generated by Dr. V. Gallo, Children's National Medical Center, Washington, DC), Cdk2 $^{-/-}$ null (generated by Dr. P. Kaldis, Institute of Molecular and Cell Biology, Singapore), 129-Cdkn1b ^{tm1Mlf} later named p27 $^{-/-}$, and C57BL/6 (catalog #003122, #003548; The Jackson Laboratory) and wild-type CD1 [Crl: CD1(ICR); Charles

River] mice were maintained at Children's National Medical Center animal facility following guidelines of the Institutional Animal Care and Use Committee (Children's National Medical Center) and the National Institutes of Health. For breeding, heterozygote CNP-EGFP $^{+}$ males were backcrossed to C57BL/6 females for more than eight generations. In CNP-EGFP mice, various stages of the oligodendrocyte lineage have been visualized based on EGFP expression driven by myelin-specific 2′,3′-cyclic nucleotide 3′-phosphohydrolase (CNP) gene promoter (Belachew et al., 2003). p27 $^{-/-}$ transgenic mice were previously described (Fero et al., 1996). Mice deficient in p27 ^{Kip1} are viable, larger than normal littermates, with better-developed organs (particularly thymus and spleen), suggesting that p27 ^{Kip1} is required in many cell lineages for normal exit from the cell cycle (Fero et al., 1996; Belachew et al., 2003). Cdk2 $^{-/-}$ transgenic mice were previously described (Berthet et al., 2003). Although larger than their litter-mates, the only morphological or structural differences in their organs compared with wild-type mice are sterile gonads.

CNP-EGFP, p27 $^{-/-}$, and Cdk2 $^{-/-}$ pups [3 d of age; postnatal day 3 (P3)] were exposed to 9.5–10.5% oxygen concentration in a hypoxic chamber. Oxygen concentration was maintained and monitored continuously with the sensor inside the chamber. To maintain hypoxic conditions, nitrogen was added to displace oxygen. To optimize nutrition during hypoxia, transgenic pups were housed in the chamber with two CD1 foster mothers and their pups. At P11, mice were removed from the chamber and transferred to a room with normoxic air conditions; however, they remained with CD1 foster mothers to minimize stress. Because of the low survival rate of p27 $^{-/-}$ mice, we modified hypoxic parameters specifically for this mouse strain to maintain oxygen concentration at 12.5%. For all three strains, exposure to hypoxia lasted 8 consecutive days (P3–P11). After 11-d-old pups were removed from the chamber, the mice proceeded to the various experimental conditions at the specified time points. Time course analysis for immunohistochemistry was performed at P11 (immediately after mice were removed from the hypoxic chamber), at P18 (at 1 week recovery in normoxic conditions), and at P45 (34 d after hypoxia).

Genotyping Cdk2$^{-/-}$ and p27$^{-/-}$ mice

To breed Cdk2 $^{-/-}$ and p27 $^{-/-}$ mice, we crossed two heterozygotes. Cdk2 $^{-/-}$ newborn pups were genotyped following the procedure established by Berthet et al. (2003). Primers used in PCR were as follows: forward, 5′-CCC GTG ATA TTG CTG AAG AGC TTG GCG-3′; reverse, 5′-GGT TTT GCT GCA TGT GGG CAT GG-3′; neo, 5′-GTG ACC CTG TGG TAC CGA GCA CCT G-3′. DNA products were loaded onto 2% agarose gel to resolve the specific bands: 150 bp for wild-type mice, 500 bp for Cdk2 $^{-/-}$, and both bands for heterozygotes.

p27 $^{-/-}$ mice were genotyped following the protocol of The Jackson Laboratory. Primers used in PCR were as follows: oIMR0947, 5′-CTC CTG CCA TTC GTA TCT GC-3′; oIMR0948, 5′-CTC CTG CCA TTC GTA TCT GC-3′; oIMR6916, 5′-CTT GGG TGG AGA GGC TAT TC-3′; oIMR6917, 5′-AGG TGA GAT GAC AGG AGA TC-3′. DNA products were loaded onto 2% agarose gel to resolve the specific bands: 190 bp for wild-type mice, 280 bp for mutant, and both bands for heterozygotes. For both strains, only mutant and wild-type mice were analyzed.

Immunocytochemistry

Immunocytochemical analysis was performed at three time points: P11, P18, and P45. Time course analysis allows identification of specific stages of oligodendrocyte development vulnerable to hypoxic damage. In each experiment, normoxic mice served as controls. Hypoxic and normoxic mice were anesthetized with isoflurane and transcardially perfused

with 0.1 M PBS, pH 7.4, followed by 4% paraformaldehyde. Brains were postfixed overnight in 4% paraformaldehyde. Serial coronal and sagittal sections (50 μm) were cut using a cryostat microtome, collected in PBS, pH 7.4, and stored at 4°C until use.

Immunocytochemistry was performed on floating sections using antibodies against the following antigens: NG2, Doublecortin, GFAP, Olig2 (Millipore Bioscience Research Reagents), Ki67 (Novocastra), c-Caspase3 (Cell Signaling), CC1 (Calbiochem), S100β, BrdU (Sigma-Aldrich), myelin basic protein (MBP) (Covance), Mash1, PDGFR (both from BD Biosciences), and Iba1 (Wako). All antibody dilutions were as previously described (Aguirre and Gallo, 2004). Sections were incubated overnight at 4°C in primary antibodies diluted in 0.1 $_{M}$ PBS, pH 7.4, containing 0.1% Triton and 5% normal goat serum. Appropriate secondary antibodies were used as follows: TRITC-conjugated AffiniPure goat anti-mouse IgG (H+L), FITC-conjugated AffinitiPure goat anti-rabbit IgG, and TRITC-conjugated AffiniPure goat anti-mouse IgM (Jackson ImmunoResearch). Sections were incubated with secondary antibodies for 1 h at room temperature and mounted.

Quantitative cellular and biochemical analysis

We used a confocal LSM (Zeiss 510) optical (magnification, 40×; step size, 1 μm) of 20- to 30-μm-thick immunostained tissue sections with a volume of 225 × 225 × 10 μm (*x*, *y*, *z*). The stacks were then *z*-axis collapsed, allowing us to analyze all elements of the cellular morphology and localize fluorescent labels to specific compartments. Four different lasers were used to image localization of FITC (488 nm excitation), CY3 (580 nm excitation), CY5 (647 nm excitation), and DAPI (400 nm excitation).

Analysis of the white matter was performed in three different areas: corpus callosum, external capsule, and cingulum. The analysis was limited within the boundaries of the white matter, as detected by DAPI distribution, to account for changes in white matter volume after hypoxia. Consistent imaging of all tissue sections and high number of sections (15–25 per group per antigen) used for quantification contributed to minimize bias. Total and relative numbers of cells expressing different antigens were estimated by scoring the number of cells double-labeled with the markers. Data were usually obtained from at least five to eight tissue sections from three to four mice per group. For CNP-EGFP mice, results are presented as mean ± SEM, and *t* tests were performed to establish statistical significance. In Cdk2 $^{-/-}$and p27 $^{-/-}$ mice, statistical analysis used two-way ANOVA to determine significant differences in oligodendrocyte proliferation and differentiation.

Western blot analysis and immunoprecipitation

White matter and SVZ areas were precisely dissected from 300-μm-thick, coronal sections from hypoxic and normoxic CNP-EGFP and p27 $^{-/-}$ mice at P11, P18, and P45. Tissues were homogenized in RIPA lysis buffer with proteinase inhibitors (Santa Cruz Biotechnology). Protein extracts were boiled for 5 min before loading onto 4–20% gradient gels (GeneMate; 20 μg of protein per lane). Gels were electrotransferred to a 0.2 μm nitrocellulose membrane (Millipore). Blots were blocked in 5% milk in TBST for 1 h, then incubated at 4°C overnight with one of the following antibodies: anti-Cdk2, -Cdk4, -cyclin E, -p27 ^{KIP1}, -MBP, -MAG (Santa Cruz Biotechnology), -Rb, -pRb(Ser780), -pRb(Ser795), -pRb(Ser807/811), -E2F1, -p107, -E2F4, -FoxO1, -FoxO3a, -FoxO4, -Skp2 (Cell Signaling), -myelin oligodendrocyte glycoprotein (MOG), -proteolipid protein (PLP) (Abcam), -Neurofilament 200 (NF200) (Sigma-Aldrich), Neurofilament H Nonphosphorylated (SMI32; Covance), and -actin (Millipore Bioscience Research Reagents; MAB). Bands were detected with appropriate horseradish peroxide-conjugated secondary antibodies, reacted with chemiluminescent ECL substrate (GE Healthcare), and visualized by x-ray exposure. Band intensity was measured using the ImageJ program (NIH). Western blots were obtained

from white matter and SVZ from three to four animals in each group and age. Data were averaged and represented as means ± SEM.

For immunoprecipitation, white matter and SVZ tissue extracts from hypoxic and normoxic CNP-EGFP mice were prepared in RIPA buffer containing 2% Triton X-100 and 0.2% SDS. Aliquots (270 μg of tissue) were incubated overnight with antibodies against E2F1 (Cell Signaling) for white matter and E2F4 (Santa Cruz Biotechnology) for SVZ, together with 15 μl of agarose A (Santa Cruz Biotechnology). Immunocomplexes bound to agarose A were collected by centrifugation and washed twice in 500 μl of RIPA buffer containing inhibitors. Precipitated proteins were analyzed by immunoblotting with an anti-Rb Abs (Cell Signaling) for white matter and anti-p107 antibody (Sigma-Aldrich) for SVZ. Bands were detected using HRP-labeled polyclonal anti-mouse Ig (BD Biosciences) and developed with a chemiluminescent substrate (ECL; GE Healthcare).

Cell culture preparation and analysis

White matter areas were dissected from 300-μm-thick coronal sections prepared from hypoxic and normoxic mice at P18 and digested for 30 min at 37°C in HBSS (Invitrogen) containing papain (13 U/ml; Sigma-Aldrich), DNase (5 U/ml; Sigma-Aldrich), and trypsin (Sigma-Aldrich). White matter cells were dissociated by trituration and resuspended in Hanks buffer containing 1 M HEPES (BioSource), 15% sucrose, and penicillin/streptavidin. For differentiation, cells were plated onto laminin-coated dishes (Invitrogen) with a density of 650 cells/μl. Equal numbers of cells from hypoxic and normoxic CNP-EGFP mice were used in all experiments. For cell differentiation assays, cells from hypoxic and normoxic white matter were cultured for 5 d and incubated with growth factors [10 μg/ml PDGF, 10 μg/ml T3 (Millipore)]. To establish the cellular composition of the cultures, we cultured white matter cells from normoxic and hypoxic CNP-EGFP mice for 24 h, and labeled them with various cell-specific markers, including MAP2 for neurons, NG2 for oligodendrocyte progenitors, GalC for mature oligodendrocytes, GFAP for astrocytes, and Iba1 for microglia. We found that neurons, astrocytes, and microglia were not affected by hypoxia and together represented a constant fraction of the total cultured cells (22.7% for normoxia and 20.9% for hypoxia). However, the percentage of mature oligodendrocytes substantially decreased after hypoxia (from 36.6 to 14.4%), while the percentage of NG2 progenitor cells increased from 40.7 to 64.7%.

To assess the proliferative potential of cells, BrdU was added to the culture medium at 10 μg/ml, followed by 60 min incubation at 37°C. Cells were then fixed in 4% paraformaldehyde and kept in PBS until use. BrdU incorporation was visualized by immunofluorescence using anti-mouse BrdU antibody and TRITC-conjugated AffiniPure goat anti-mouse IgG (H+L). To study whether proliferating cells belonged to the oligodendrocytic lineage, we costained NG2 $^{+}$, Olig2 $^{+}$, O4 $^{+}$, GalC $^{+}$, and GFAP $^{+}$ cells with anti-BrdU or anti-Ki67 antibodies. Standard protocols were used to immunolabel differentiated cells (Aguirre and Gallo, 2004) with primary antibodies against O1 (Millipore) and O4 (R&D). For quantification, the percentages of positive cells were counted in random fields captured at 10× magnification (>250 cells per condition and per stain) from at least three different samples and subjected to statistical analysis. We found that, in normoxia, mainly NG2 $^{+}$ (69.0%) and Olig2 $^{+}$ (74%) cells were proliferating in the cultures. We also found only a small fraction of GalC $^{+}$BrdU $^{+}$ (3%), O4 $^{+}$BrdU $^{+}$ (8%), GFAP $^{+}$BrdU $^{+}$ (9%), and Iba1 $^{+}$BrdU $^{+}$ (8%) cells. In hypoxia, still mainly NG2 $^{+}$ (85%) and Olig2 $^{+}$ (54%) cells were proliferating, whereas only a small fraction of GalC $^{+}$BrdU $^{+}$ (2%), O4 $^{+}$BrdU $^{+}$ (3%), GFAP $^{+}$BrdU $^{+}$(8%), and Iba1 $^{+}$BrdU $^{+}$(8%) cells were detected.

Retroviral injection of p27^{Kip1} into white matter

Dividing cells in white matter were directly labeled with CMV-GFP retrovirus in hypoxic and normoxic brains at P18. The virus plasmid pNIT contains a cDNA fragment of EGFP downstream of the tetracycline operon enhancer-promoter. For *in vivo* experiments, wild-type mice (P18) were stereotaxically injected in the white matter with p27 ^{Kip1} EGFP retrovirus stock (2 μl; titer, 1–2 × 10 ^{6} cfu ml $^{-1}$). For a control, mock virus was injected into white matter. The following coordinates were used: 1 mm anteroposterior, 1 mm mediolateral, and 1.5 mm dorsoventral. Brains were processed for immunohistochemical staining using anti-CC1 (Calbiochem) and S100β antibodies (Sigma-Aldrich).

Electron microscopy

For ultrastructural investigation of myelinated axons in hypoxic and normoxic white matter, brains from P18 and P45 mice were perfused with 4% paraformaldehyde containing 15% picric acid and 0.2% glutaraldehyde. After washing in 0.1 M PBS, brains were sectioned at 200 μm on the vibratome. Sections were osmicated 60 min in 1% osmium tetroxide (Electron Microscopy Sciences) in 0.1 M phosphate buffer, washed several times in distilled water, contrast enhanced for 30 min with 1% uranyl acetate (Electron Microscopy Sciences), and dehydrated in ascending concentrations of acetone. Finally, sections were soaked 60 min in a mixture of Araldite 502 (5.4 g), DDSA (4.6 g), DMP-30 (0.2 g) (all from Electron Microscopy Sciences), and flat-embedded between glass slides and coverslips at 65°C for 48 h. Prepared sections were cut into semithick sections (90 μm), stained with toluidine blue for anatomical identification of white matter, and resectioned into 70 nm ultrathin sections. These sections were examined with a JEOL transmission electron microscope (JEM-1400), and pictures were taken with a Gatan SC1000 ORIUS CCD camera. Electron-microscopic images were prepared using Adobe Photoshop CS2.

siRNA-induced FoxO1 and Skp2 knockdown in white matter cells

Cell transfection was performed using the NeuroPORTER Transfection Reagent (Genlantis, T400750) according to the manufacturer's instructions. After white matter dissection, cells were plated in 12-well cell culture dishes at a density of 50 cells/μl for 24 h. At the time of transfection, cell cultures were ~60% confluent. Commercially available siRNAs directed toward FoxO1 and Skp2 were purchased from Dharmacon. A mixture of siRNAs (20 p_M each) produced specific knockdown of FoxO1 and Skp2 at 7 h after transfection. Briefly, 2 μl of 20 p_M of each FoxO1 or Skp2 siRNA solution and 12 μl of the transfection reagent were incubated in 100 μl of OptiMEM medium (Invitrogen) for 20 min, to facilitate complex formation. The siRNA transfection mix was added to the cells cultured in 10% FBS. Control consisted of nonspecific siRNA (Silencer negative). Cells were transfected for 7 h at 37°C, washed with Hanks buffer, and cultured in MEM with 10% FBS for an additional 24 h. The medium was then changed to stem cell medium (SCM) (20 ng/ml EGF and 10 ng/ml FGF), and cells were cultured for 4 d. To assess the proliferative potential of cells, BrdU was added to the culture medium at a concentration of 10 μg/ml, followed by 60 min incubation at 37°C. Cells were then fixed in 4% paraformaldehyde and kept in PBS until use. BrdU incorporation was visualized by immunofluorescence using anti-mouse BrdU antibody. Percentages of BrdU $^{+}$ cells were quantified from at least three different experiments and subjected to statistical analysis. To demonstrated FoxO1 and Skp2 knockdown, Western blots analysis was performed on transfected CNP-EGFP cells from normoxic and hypoxic mice. After transfection, cells were lysed in 50 μl of ice-cold RIPA buffer. Protein samples were prepared and processed as described in Western blots analysis and immunoprecipitation. Membranes were incubated with anti-FoxO1, anti-Skp2, and anti-p27 ^{Kip1} antibodies, and results were normalized relatively to actin.

Overexpression of p27^{Kip1} and FoxO1 in white matter cells

To overexpress p27 ^{Kip1} or FoxO1 in white matter cells from normoxic and hypoxic brains at P18, we used a p27 ^{Kip1} retrovirus (a gift from Dr. M. Luskin, Emory University, Atlanta, GA) or mock virus and pCMV5 HA FoxO1 plasmid (Addgene), or an empty vector as a control. Plasmid constructs were introduced into cultured cells by liposomal transfection for 6 h in 12-well plates using 1.0 μg of DNA and 12 μl of NeuroPORTER Transfection Reagent in OptiMEM medium. After transfection, the cells were washed in SCM containing 20 ng/ml EGF and 10 ng/ml FGF, and plated for poly-lysine-coated dishes for culturing. After 5 d in culture, cells were labeled with anti-O4, -O1, -GalC, -Olig2, and -p27 ^{Kip1} antibodies or collected for Western blot. Membranes were incubated with anti-FoxO1 and anti-p27 ^{Kip1} antibodies, and results were normalized relatively to actin.

All human tissue was collected in accordance with guidelines established by the University of California San Francisco Committee on Human Research (H11170-19113-07) (Table 1). Following autopsy, all brains, except case 2, were immersed in PBS with 4% paraformaldehyde for 3 d. On day 3, the brain was cut in the coronal plane at the level of the mamillary body and immersed in fresh 4% paraformaldehyde/PBS for an additional 3 d. In case 2, the brain was immersed in 4% phosphate-buffered formalin for 1 week at room temperature. After fixation, all tissue samples were equilibrated in PBS with 30% sucrose for at least 2 d. Following sucrose equilibration, tissue was placed into molds and embedded with OCT for 30 – 60 min at room temperature or 4°C followed by freezing in dry ice-chilled ethanol or methyl butane. The diagnosis of hypoxic ischemic encephalopathy (HIE) requires clinical and pathological correlations. With respect to the pathological features, all HIE cases in this study showed consistent evidence of diffuse white matter injury, including astrogliosis and macrophage infiltration. These findings were confirmed by the increase in the number and the staining intensity of GFAP- or CD68-positive cells, respectively. In addition, the HIE case also showed evidence of neuronal injury, including the presence of ischemic neurons and variable degrees of neuronal loss, in cerebral cortex, hippocampus, and basal ganglia.

Cases 1 and 2 demonstrated clinical evidence of HIE and pathological evidence of HIE and low output state in multiple organs on postmortem examination. More specific findings in case 1 (8 weeks of age, born at full term) included hypoplastic left heart status-post procedure and diffuse white matter injury in brain with focal neuron dropout in cerebral and cerebellar cortices. Case 2 (5 months of age, born prematurely at 26 weeks gestation) with a clinical diagnosis of severe HIE who underwent therapeutic hypothermia showed diffuse white matter injury on postmortem evaluation. Case 6 (1-d-old term infant) with midgut volvulus with extensive hemorrhagic necrosis of small bowel was not found to have significant neuropathological findings of HIE.

RT-PCR

cDNA was first synthesized from 1.5 to 2 μg of total RNA extracted from cultured cells obtained from hypoxic and normoxic white matter in a total volume of 11 μl, including 10 m_M dNTP mix and 0.5 μg/μl oligo-dT (Invitrogen; 12371-019). Reaction mixtures were heated at 65°C for 5 min, and then at 42°C for 50 min. From 2 μl of cDNAs, sequences of interest were amplified in a thermocycler in a total volume of 25 μl of mixture with Taq polymerase. Primer pairs are described in the supplemental materials. PCR products were resolved by vertical electrophoresis on 2% agarose gels. Intensity of bands was measured using the Image J program (NIH). Primers were as follows: CNP, 5′-CCG GAG ACA TAG TGC CCG CA-3′; 5′-AAA GCT GGT CCA GCC CTT CC-3′; MBP, 5′-CTA CCC ACT GTC GAT GAC TTA TTG ATT AGA C-3′; 5′-CTC TAA TCA ATA AGT CAT CGA CAG TGG GTA C-3′; Olig2, 5′-GTG TCT AGT CGC CCA CGT G-3′; 5′-CGA TGT

TGA GGT CGT GCA T-3′; GFAP, 5′-ACT TAA CAA ATC CCT TCC TTC ATC C-3′; 5′-CCC TCT CTC CTG TTC AGT G-3′; Actin, 5′-CGT GGG CCG CCC TAG GCA CA-3′; 5′-TTG GCC TTA GGG TTC AGG GGG-3′.

Results

Neonatal hypoxia exerts a biphasic effect on oligodendrocyte and white matter development

In prematurely born infants, the highest risk for DWMI occurs around 23–32 weeks of gestation, corresponding to the onset of premyelinating oligodendrocyte (pre-OL) production and early white matter myelination. DWMI involves substantial reduction in the number of mature oligodendrocytes (Back et al., 2001). Recent work indicates that, following such injuries in humans and rodent models, immature OPCs can repopulate such lesions, but they appear to be blocked at an immature state of differentiation (Buser et al., 2012; Back et al., 2001; Billiards et al., 2008). To study the effect of hypoxia on oligodendrocyte development in a DWMI mouse model, we exposed CNP-EGFP mice (a mouse strain in which EGFP is selectively expressed in oligodendrocyte lineage cells) (Belachew et al., 2003; Aguirre et al., 2007) to hypoxic conditions (9.5–10.5% O_2) from P3 through P11. We initially performed Western blot and immunocytochemical analysis at P11, P18, and P45, to analyze myelin protein expression. Western blots showed that hypoxia did not modify MBP and CNP expression in white matter at P11. However, at P18, levels of both proteins were significantly reduced, as was the width of the subcortical white matter (30.74 ± 4.41% decrease; $n = 4$; $p < 0.05$). After long-term recovery in normoxia (P45), expression of both markers was upregulated (Fig. 1 *A*–*C*). A similar developmental pattern was observed for other myelin proteins, including MAG, PLP, and MOG, demonstrating reduced levels at P18, followed by an increase at P45 (Fig. 1 *B*, *C*). PLP expression was upregulated after hypoxia at P11, suggesting degenerative changes in axons.

Immunohistochemical analysis of oligodendrocyte lineage cells confirmed the biochemical results. CNP-EGFP $^+$ cells were labeled with anti-CC1 (mature oligodendrocytes) and anti-Olig2 (all oligodendrocyte lineage cells). At P11, hypoxia caused no significant changes in the density of CNP-EGFP $^+$cells expressing these markers in corpus callosum. However, 1 week after hypoxic insult (P18), we observed significantly fewer mature oligodendrocytes expressing CC1 and Olig2; and by P45, long-term recovery in normoxic conditions resulted in significantly more CNP-EGFP $^+$CC1 $^+$and CNP-EGFP $^+$Olig2 $^+$cells in white matter of hypoxia reared mice, compared with white matter of normoxic mice (Fig. 1 *D*–*G*).

To further investigate whether the biphasic changes in myelin protein levels were due to alterations in the number of oligodendrocytes, we quantified CNP-EGFP $^+$ cells in white matter of normoxic and hypoxic CNP-EGFP mice, demonstrating a transient reduction of total CNP-EGFP $^+$ cells after hypoxia at P18 (by 31.1 ± 2.5%), followed by an increase at P45 (35.3 ± 3.9%).

Furthermore, to determine whether hypoxia-induced reduction in the number of mature white matter oligodendrocytes at P18 was due to apoptosis, CNP-EGFP $^+$ cells were stained for Caspase 3 at different intervals after hypoxia. Consistent with the oligodendrocyte numbers, the number of Caspase 3$^+$CNP-EGFP $^+$ cells was significantly increased at P11 and P18, but no changes in cell death were detected at P45 after long-term recovery in normoxia (Fig. 2 *A*, *B*). Importantly, after hypoxia, 100% of Caspase 3$^+$CNP-EGFP $^+$ cells were CC1$^+$ oligodendrocytes and no Caspase-3-negative CNP-EGFP $^+$ cells were detected (Fig. 2*C*).

Although significant oligodendrocyte death occurs within the first week after hypoxia, our results indicated that both myelin protein levels and total number of oligodendrocytes are fully recovered 1 month after hypoxia. This suggested that new oligodendrocytes are being generated during this time period. To determine whether hypoxia promotes oligodendrogenesis, hypoxic and normoxic mice received five intraperitoneal injections of BrdU at 12 h intervals, starting on P11. At P45, CNP-EGFP $^{+}$ cells were stained for BrdU and colabeled with anti-CC1 and anti-S100β antibodies. Cellular analysis demonstrated a twofold increase in the total number of CNP-EGFP $^{+}$BrdU $^{+}$ oligodendrocytes and in the number of CNP-EGFP $^{+}$CC1 $^{+}$ and CNP-EGFP $^{+}$S100β^{+} cells (Fig. 3*A–C*) in hypoxic compared with normoxic mice, indicating the generation of new oligodendrocytes during the first week following hypoxic insult.

The results above indicate that long-term cellular (oligodendrocytes) and biochemical (myelin proteins) recovery appears to occur in white matter after hypoxia. To determine whether cellular recovery leads to proper myelin production and axonal myelination, we performed electron-microscopic analysis of white matter at different intervals after hypoxia. At P18, hypoxia caused a reduction in relative myelin thickness, as determined by an increase in *G* ratio (axon diameter divided by entire myelinated fiber diameter; normoxia: 0.79 ± 0.009, $n = 49$ axons; hypoxia: 0.88 ± 0.007, $n = 38$ axons). Consistent with the observation that at P45 MBP levels and the total number of oligodendrocytes both recovered after hypoxia (Fig. 1 *E*, *F*), at this age, relative myelin thickness was increased after hypoxia, compared with normoxia (*G* ratio; normoxia: 0.87 ± 0.007, $n = 56$ axons; hypoxia: 0.79 ± 0.006, $n = 42$ axons) (Fig. 4 *A*, *B*). However, hypoxic injury did not interact with the age of mice, resulting in a comparable reduction of myelinated axons at both P18 and P45 by 12 and 14%, respectively. Furthermore, in hypoxia, we also observed a decrease in axonal diameter in both age groups [P18: 0.67 ± 0.04 μm (normoxia), 0.47 ± 0.11 μm (hypoxia); P45: 0.78 ± 0.03 μm (normoxia), 0.41 ± 0.03 μm (hypoxia)]. Also, electron-microscopic analysis indicated that axons are loosely wrapped by partially delaminated myelin sheaths after hypoxia (Fig. 4 *A*), although the expressions of total neurofilament (NF200) and nonphosphorylated neurofilament (SMI32) proteins remain unchanged at P18 and P45 [for NF200, at P18: 2.13 ± 0.2% decrease; at P45: 0.56 ± 0.27% increase; for SMI32, at P18: 1.42 ± 0.15 decrease; at P45: 2.66 ± 0.37% decrease ($n = 3$ for each group, for each condition) (Fig. 4*C*)].

Neonatal hypoxia causes a regenerative OPC response in white matter and SVZ

We first characterized the time course of OPC proliferation after hypoxia in both white matter and SVZ, the two regions containing the largest numbers of progenitor cells capable of regenerating oligodendrocytes (Menn et al., 2006; Aguirre et al., 2007). To assess OPC proliferation after hypoxia, we performed anti-Ki67 immunostaining of normoxic and hypoxic white matter and SVZ at three time points during development. In white matter, CNP-EGFP $^{+}$Ki67 $^{+}$cells showed a greater proliferative response during the first week after hypoxia (P11 and P18), whereas no hypoxia-induced cell proliferation was detected at P45 (Fig. 5*A*, *B*). At P11, we also observed a fourfold increase in CNP-EGFP^{+}NG2 $^{+}$and a threefold increase in CNP-EGFP^{+}NG2 $^{+}$Ki67 $^{+}$cells after hypoxia, compared with normoxia. This effect was still present at P18, but no significant differences were observed at P45 (Fig. 5*C–E*). Changes in microglia and astrocyte proliferation were not detected in white matter after hypoxia, as determined by anti-BrdU and -Ki67 immunostaining of Iba1- and GFAP-expressing cells, respectively (Fig. 6*A–C*) (Raymond et al., 2011).

In brains exposed to hypoxia, we consistently observed considerable expansion of the SVZ, together with lateral ventricle enlargement (Fig. 7*A*). Cellular analysis using anti-Ki67 immunostaining attributed this effect to a large and significant increase in overall SVZ cell proliferation, which— differently from white matter—persisted even after long-term

recovery in normoxia at P45 (Fig. 7*B*). We characterized hypoxia-induced changes in the SVZ progenitor population using neuronal and oligodendrocytic progenitor markers. At P18, we detected an increased number of CNP-EGFP $^{+}$ cells expressing either Dcx (neuronal), or NG2, or Olig2, or Mash1 (oligodendrocyte) progenitors, which persisted at P45 after long-term recovery in normoxia (Fig. 7*C–E*).

These results demonstrate that OPCs proliferate in response to hypoxia in both white matter and SVZ, with the regenerative response occurring in both regions within a week after injury. Importantly, in the SVZ, this OPC response persists 1 month after hypoxia, suggesting that these cells may contribute to white matter repair for extended periods following injury.

Distinct cell cycle pathways regulate cell proliferation in white matter and SVZ after neonatal hypoxia

Our biochemical and cellular analyses demonstrate that, despite a proliferative and regenerative response of white matter and SVZ OPCs after hypoxia, oligodendrocyte maturation is delayed, leading to hypomyelination. As our findings highlight the importance of identifying factors that promote timely oligodendrogenesis after hypoxia, we investigated the cell cycle pathways involved in regulating OPC proliferation and differentiation in white matter and SVZ after hypoxia.

We performed extensive Western blot analysis of cell cycle proteins that regulate G_1–S transition in OPCs (Casaccia-Bonnefil et al., 1997; Durand et al., 1997; Tikoo et al., 1998; Ghiani and Gallo, 2001; Nguyen et al., 2006), and compared hypoxic and normoxic white matter, as well as SVZ tissue, at P18. In white matter, hypoxia up-regulated Cdk2, pRb807/811, cyclin E, E2F1 expression compared with normoxia, and concomitantly downregulated $p27^{Kip1}$ (Fig. 8 *A–C*). Furthermore, p53 expression was also increased (45.04 ± 5.9% increase), whereas $p21^{Cip1}$ was downregulated after hypoxia (39.1 ± 5.4% decrease). In the SVZ at P18, hypoxia caused increased Cdk4, p107, and E2F4 protein levels compared with normoxia (Fig. 8 *A–C*), suggesting that the Cdk4 pathway may regulate hypoxia-induced OPC proliferation in the SVZ. Our results suggest that, after hypoxia, distinct cell cycle pathways—Cdk2 and Cdk4 —regulate the OPC proliferative response in white matter and SVZ, respectively.

To analyze functional activation of the Cdk2 and Cdk4 pathways in these regions, we coimmunoprecipitated pocket proteins (Rb and p107) with their respective transcription factors (E2F1 and E2F4). Cdk2 phosphorylates the Rb–E2F1 complex causing its dissociation, while Cdk4 has a similar effect on the p107–E2F4 complex (Beijersbergen et al., 1995). Lower levels of Rb–E2F1 complex were detected in hypoxic, compared with normoxic, white matter (Fig. 8 *D*), indicating a higher fraction of unbound E2F1. Increased E2F1 promotes the entry of cells into the S phase of the cell cycle, resulting in increased proliferation. In hypoxic SVZ, a reduction in p107–E2F4 was detected, indicating higher levels of unbound E2F4 protein as a mechanism underlying increased SVZ cell proliferation. Regional specificity of Cdk2 and Cdk4 in cell proliferation was demonstrated by finding that the Rb–E2F1 complex and the p107–E2F4 complex were elevated in the SVZ and in white matter after hypoxia, respectively (Fig. 8 *D*), confirming that these pathways were not involved in hypoxia-induced progenitor proliferation in these regions.

Analysis of Cdk2 $^{-/-}$ mice further substantiated Cdk2 pathway involvement in hypoxia-induced cell proliferation in white matter. Cdk2 $^{-/-}$mice and their wild-type littermates were compared at P18 and P45 (Fig. 9*A–F*). In Cdk2 $^{-/-}$ mice, at P18, hypoxia caused only a modest elevation in the number of Ki67 $^{+}$ cells in white matter, whereas a proliferative effect remained pronounced in the SVZ (Fig. 9 *A*, *B*). The proliferative index was

significantly lower in Cdk2 $^{-/-}$ white matter than in their wild-type littermates after hypoxia. At P18, in white matter of Cdk2 $^{-/-}$ mice, 74 ± 1.4% of the Ki67 $^{+}$ cells were NG2 $^{+}$ and 100% were Olig2 $^{+}$. Additionally, in Cdk2 $^{-/-}$ mice, hypoxia still affected oligodendrocyte differentiation in white matter, as demonstrated by reduced numbers of Olig2 $^{+}$ and CC1 $^{+}$ cells at P18, followed by an increase of their numbers at P45 (Fig. 9*C–F*). These data indicate that Cdk2 is an essential kinase, controlling OPC proliferation in white matter after hypoxia.

FoxO1 and Skp2 regulate p27 ^{Kip1} expression after neonatal hypoxia

Our results demonstrate hypoxia-induced changes in several cell cycle proteins in white matter, including p27 ^{Kip1}, p21, and p53. In this study, we focused on p27 ^{Kip1} as a potential enhancer of oligodendrocyte regeneration after DWMI, based on its role in oligodendrogenesis under physiological conditions (Casaccia-Bonnefil et al., 1997). Consistent with the Western blot results, immunocytochemical analysis of p27 ^{Kip1} expression in the CNP-EGFP mouse demonstrated that hypoxia first caused a reduction in the percentage of CNP-EGFP $^{+}$ cells expressing p27 ^{Kip1} and of Olig2 $^{+}$p27 $^{Kip1+}$ cells at P18, followed by an increase at P45 (Fig. 10 *A–C*). The percentage of these cells was not different from normoxic controls at P11 (Fig. 10 *B*, *C*). We next validated these observations using human neonatal tissue. In subcortical white matter of full-term neonates with hypoxic–ischemic encephalopathy versus controls, we observed a significant reduction in p27 $^{Kip1+}$Olig2 $^{+}$ cells (Fig. 10 *D–F*), indicating that p27 ^{Kip1} expression is also downregulated in human OPCs after hypoxic injury.

Interestingly, in mouse white matter, Cdk2 and p27 ^{Kip1} levels displayed reciprocal expression patterns during development, with maximal Cdk2 expression at P18 when p27 ^{Kip1} expression is lowest (Fig. 11 *A*, *B*). It has been shown that FoxO transcription factors control p27 ^{Kip1} expression in cancer cells (Myatt and Lam, 2007; Yang and Hung, 2009). Also, the oncoprotein Skp2 mediates degradation of several Cdk inhibitors, including p27 ^{Kip1} (Dehan and Pagano, 2005). Therefore, we first investigated whether expression of FoxO proteins—including FoxO1, FoxO3a, and FoxO4 —and of Skp2 were altered after neonatal hypoxia in a manner consistent with a putative regulatory role. Western blot analysis demonstrated similar developmental patterns of expression of the FoxO proteins in white matter after hypoxia (Fig. 11 *A*, *B*). Expression of these transcription factors was not modified immediately after hypoxia at P11. At P18, hypoxia caused a significant reduction in the expression of FoxO1, FoxO3a, and FoxO4, compared with normoxic white matter (Fig. 11 *A*, *B*). Conversely, at P45 all FoxO proteins analyzed were up-regulated after hypoxia (Fig. 11 *A*, *B*). Additionally, we observed that expression of Skp2 was increased after neonatal hypoxia, resulting in higher levels at P11 and P18. Importantly, hypoxia caused no change in Skp2 expression at P45, when FoxO protein levels were drastically increased. However, consistent with a role of Skp2 in p27 ^{Kip1} degradation, Skp2 expression levels were inversely related to p27 ^{Kip1} in hypoxic white matter at P18 (Fig. 11 *A*, *B*). Together, these data indicate that degradation of p27 ^{Kip1}, as manifested by lower protein levels, was likely mediated by Skp2 and involved FoxO transcription factors.

To study whether FoxO1 knockdown mimicked the effect of hypoxia on oligodendrocyte differentiation, we first performed loss-of-function experiments, where siRNA-mediated FoxO1 knockdown was induced in white matter cells isolated from normoxic brains. Transfection with FoxO1 siRNA significantly decreased FoxO1 (65.20 ± 2.1%) and p27 ^{Kip1} (94.11 ± 1.5%) expression, compared with cells transfected with scrambled control (Fig. 11*C*). Normoxic cells transfected with FoxO1 siRNA generated less oligodendrocytes expressing p27 ^{Kip1}, O4, GalC, and Olig2, and more BrdU $^{+}$ cells, compared with white matter cells transfected with scrambled control (Fig. 11 *D*). Conversely, in gain-of-function experiments, where FoxO1 was overexpressed in cells isolated from hypoxic white matter

(Fig. 11 *E*), we observed a significant increase in the percentage of oligodendrocytes, compared with cells transfected with empty vector (Fig. 11 *F*). Overexpression of FoxO1 also significantly reduced BrdU $^{+}$ cells in hypoxic culture (Fig. 11 *F*).

To study whether Skp2 was functionally involved in p27 ^{Kip1} degradation after hypoxia, we performed knockdown of Skp2 in white matter cells after normoxia and hypoxia, respectively (Fig. 11*G*). In cells isolated from normoxic white matter, Skp2 knockdown did not significantly change the number of oligodendrocytes, compared with control cultures (Fig. 11 *H*). Conversely, in cells isolated from hypoxic white matter, transfection with Skp2 siRNA increased the percentages of p27 $^{Kip1+}$, O4 $^{+}$, GalC $^{+}$, and Olig2 $^{+}$ cells, compared with cells transfected with scrambled control (Fig. 11 *H*). Finally, proliferation assays demonstrated that Skp2 knockdown caused a reduction in the percentage of BrdU $^{+}$ cells, compared with cells transfected with scrambled control (Fig. 11 *H*). Together, these data indicate that FoxO1 and Skp2 functionally contribute to the changes in p27 ^{Kip1} expression in white matter after hypoxia.

p27 ^{Kip1} plays an important role in oligodendrocyte differentiation after neonatal hypoxia

Our analysis of white matter after hypoxia indicates a correlation between reduced number of mature oligodendrocytes, myelin expression, and concomitant FoxO1-dependent reduction in p27 ^{Kip1} expression. Therefore, we hypothesized that reduced p27 ^{Kip1} levels during a critical developmental time window after hypoxia would prevent oligodendrocyte differentiation, and tested our hypothesis using a loss- and gain-of-function approach.

We exposed p27 $^{-/-}$ mice to hypoxia and performed immunocytochemical analysis of white matter and SVZ at P18. As in their wild-type littermates, p27 $^{-/-}$ mice displayed enhanced cell proliferation in the SVZ after hypoxia, revealed by Ki67 and BrdU immunostaining. This effect was more pronounced in p27 $^{-/-}$ than in wild-type littermates (Fig. 12 *A*–*D*). Along with a higher proliferative rate, p27 $^{-/-}$ mice displayed structural expansion of the SVZ after hypoxia compared with normoxia. Moreover, the relative increase in SVZ NG2 $^{+}$ and Olig2 $^{+}$ cells induced by hypoxia was higher in p27 $^{-/-}$ than in wild-type mice (Fig. 12 *B*–*D*). However, in white matter of p27 $^{-/-}$ mice, hypoxia caused a larger reduction in the number of Olig2 $^{+}$ (63.7 ± 5.43% decrease; $n = 3$; $p < 0.05$), CC1 $^{+}$ (71.03 ± 9.7% decrease; $n = 3$; $p < 0.05$), and S100β^{+} (82.92 ± 0.2% decrease; $n = 3$; $p < 0.05$) cells than in wild-type mice (Fig. 12 *E*, *F*,*H*). Western blots of MBP after hypoxia confirmed the immunocytochemical analysis, demonstrating a larger reduction in MBP expression in p27 $^{-/-}$ (29.2 ± 3.8%) compared with wild-type (16.0 ± 0.8%) mice ($p < 0.01$, *t* test; Fig. 12*G*,*I*). Together, these results indicate that loss of p27 ^{Kip1} exacerbates the effects of hypoxia on oligodendrocyte maturation in developing white matter.

Enhanced p27 ^{Kip1} expression restores oligodendrogenesis after neonatal hypoxia

Our loss-of-function results point to p27 ^{Kip1} as a potential target to promote oligodendrocyte differentiation after hypoxia. Therefore, we performed *in vitro* and *in vivo* gain-of-function experiments to directly demonstrate its role in oligodendrocyte regeneration after hypoxia. We first isolated white matter cells from normoxic and hypoxic mice at P18 and transfected them *in vitro* with p27 ^{Kip1}-expressing retrovirus. To assess their proliferative potential, we labeled all cultured cells with BrdU (Fig. 13 *A*, *D*). In normoxic cells, the percentage of BrdU $^{+}$cells slightly decreased after p27 ^{Kip1} transfection compared with cells transfected with control virus. In cells isolated from hypoxic mice, p27 ^{Kip1} overexpression caused a more pronounced inhibitory effect on cell proliferation (Fig. 13*A*–*D*).

Consistent with its effects on cell proliferation, p27 ^{Kip1} overexpression also enhanced oligodendrocyte differentiation in cells isolated from hypoxic mice. The percentage of O4 $^{+}$ and O1 $^{+}$ cells was strongly enhanced (4-fold increase of O4 $^{+}$cell number, and a 2.5-fold increase in O1 $^{+}$ cells) in cells isolated from hypoxic mice after p27 ^{Kip1} transfection, compared with mock-transfected cells; p27 ^{Kip1} overexpression did not affect oligodendrocyte differentiation in cells isolated from normoxic mice (Fig. 13*B–D*). These immunocytochemical results were confirmed by semiquantitative RT-PCR analysis demonstrating increased *CNP*, *MBP*, and *Olig2* gene expression in hypoxic cells transfected with p27 ^{Kip1}, compared with cells treated with mock virus or normoxia, whereas expression of *GFAP* remained unchanged (data not shown). Furthermore, Western blot analysis demonstrated reduced protein expression of Cdk2 and E2F1, as well as increased MBP protein expression in hypoxic cells transfected with p27 ^{Kip1} (data not shown). Conversely, Cdk2, E2F1, and MBP expression were not modified by p27 ^{Kip1} in normoxic cells (data not shown).

To demonstrate that p27 ^{Kip1} overexpression enhances OPC differentiation after hypoxia *in vivo*, we injected p27 ^{Kip1} and mock EGFP-retrovirus into hypoxic and normoxic white matter of wild-type mice at P18. Three weeks later, we labeled brain sections with anti-Olig2, -CC1, -S100*β*, and -MBP antibodies. Because p27 ^{Kip1} retrovirus mainly targets proliferating cells, a larger number of EGFP-labeled cells incorporating the retrovirus were found in hypoxic than in normoxic white matter, indirectly confirming enhanced proliferation after hypoxia (data not shown). p27 ^{Kip1} injection caused a significant increase in the number of oligodendrocytes expressing CC1, S100*β*, and Olig2 in hypoxic white matter, compared with mock-injected hypoxic white matter cells (Fig. 13*E–G*, *I–K*). A significant percentage (45.0 ± 7.05%) of p27-virus $^{+}$ cells were also MBP $^{+}$ (Fig. 13 *H*, *L*). In normoxic white matter, no mature oligodendrocytes were detected after mock transfection, and p27^{Kip1} overexpression caused a modest increase in the number of mature oligodendrocytes, similar to that found in mock-injected brains (Fig. 13*I–L*). Together, these results directly demonstrate that restoring p27^{Kip1} expression in white matter OPCs after hypoxic neonatal brain injury promotes oligodendrocyte differentiation.

Discussion

Using an animal model relevant to DWMI observed in preterm infants, our study identifies two distinct developmental phases: an injury phase occurring within a few days after hypoxia, and a phase of apparent cellular and biochemical recovery within a few weeks after hypoxia. These two phases have also been observed in premature infants during their postnatal development (Back et al., 2001; Volpe, 2001). We identify a developmental time window during oligodendrogenesis that is critical for proper white matter myelination, as hypoxic insult during this period produces transient hypomyelination and failure of functional recovery. Our analysis also demonstrates that hypoxia affects oligodendrogenesis and oligodendrocyte differentiation through two crucial cell cycle proteins, Cdk2 and its inhibitor p27^{Kip1}.

White matter displays a biphasic response to neonatal hypoxia

We demonstrate that neonatal hypoxia causes transient hypomyelination due to significantly increased oligodendrocyte cell death and delayed oligodendrocyte differentiation. One week after hypoxia, the main populations affected comprised CC1 $^{+}$ mature oligodendrocytes, which are normally involved in myelination. The reduction in mature oligodendrocytes decreased the expression of myelin proteins, likely as a result of both oligodendrocyte death and delayed oligodendrocyte maturation. Previous studies have shown that oligodendrocyte depletion after hypoxia–ischemia is caused by degeneration of O4 $^{+}$ preoligodendrocytes and by arrested oligodendrocyte maturation at a premyelinating developmental stage (Ness

et al., 2001; Back et al., 2002). Our study demonstrates an increased number of Caspase-3 $^{+}$ oligodendrocytes the first week after hypoxic insult, but this was not sustained for a longer period after hypoxia. This finding is consistent with the recovery of myelin protein levels a week after hypoxia.

We also demonstrate that, in white matter, the strongest proliferative response of NG2 $^{+}$-expressing progenitors occurs the first week after the hypoxic insult, suggesting short-term oligodendrocyte regeneration. In our model, exposure to low oxygen for 8 d caused increased proliferation of SVZ progenitors expressing NG2, Mash1, and Olig2, which persisted at least 2 weeks longer in the SVZ than in white matter, demonstrating a differential response to injury in these progenitor populations.

We followed the complete developmental time course, analyzing the effects of low oxygen on the oligodendrocyte lineage up to P45—the age corresponding to complete myelination. We show that sublethal hypoxia affects oligodendrogenesis within the first week after the insult during developmental myelination, a process then followed by oligodendrocyte regeneration from proliferating NG2 $^{+}$progenitors. These data suggest that juvenile white matter has an endogenous potential for cellular recovery after chronic hypoxic injury. This conclusion is consistent with observations after DWMI in adolescent human brain, demonstrating white matter recovery accompanied by partial functional improvement (Ment and Constable, 2007). Reconstitution of oligodendrocyte cell number in hypoxic white matter is also consistent with recent studies that demonstrated a similar course of regenerative events in cortical neurogenesis after hypoxia (Fagel et al., 2009). Together, these findings indicate a general pattern of brain recovery following hypoxic insult, involving both neurogenesis and oligodendrogenesis with similar time courses. Our study found oligodendrocyte regeneration underway as early as within the first week after hypoxia. However, this regenerative event was not accompanied by proper developmental myelination—indicating that hypoxia induces delayed oligodendrocyte maturation. One month after injury, the cellular and biochemical recovery (higher number of oligodendrocytes and higher levels of myelin protein expression at P45) was not fully reflected by normal axonal myelination (lower *G* ratio) revealed by electron microscopy. Also, we did not observe changes in the expression of axonal neurofilaments, suggesting that at this time point axonopathy does not play a crucial role in the observed effects on oligodendrocytes. Importantly, the present study identifies a developmental time window critical for myelination, which could be targeted in new therapies for preventing white matter defects during development. When oligodendrocyte maturation and myelination are prevented during this specific time window, disordered white matter function in adulthood will ultimately result.

Cdk2 and Cdk4 pathways regulate proliferation of different progenitor populations

Building on the distinctive time course of the cellular response of white matter and SVZ progenitor cells to hypoxia, we examined differential expression of cell cycle regulatory proteins in these regions. Our analysis demonstrates that two distinct signaling pathways regulate the proliferative response of two different progenitor populations to hypoxia, in particular the Cdk2 pathway in white matter and the Cdk4 pathway in SVZ. Furthermore, we show that the Cdk2 pathway is functionally involved in OPC proliferation in white matter, whereas hypoxia-induced progenitor proliferation in the SVZ is controlled by activation of the Cdk4 pathway, since in white matter— but not in SVZ—OPC proliferation induced by hypoxia was abolished in a Cdk2-null mouse. The Cdk2 pathway is known to regulate OPC proliferation during development (Krtolica et al., 1998; Ghiani et al., 1999; Gardner et al., 2001; Belachew et al., 2003; Caillava et al., 2011). Our study reveals upregulation of each component of the Cdk2 pathway—including Cdk2, Rb807/811, and E2F1 proteins—in hypoxic white matter. We also provide evidence for functional activation

of the Cdk2 pathway as a crucial regulator of OPC proliferation under pathological conditions, DWMI in particular. Cdk2 deletion also severely impairs oligodendrocyte regeneration and remyelination after focal demyelination of adult white matter (Caillava et al., 2011), indicating that Cdk2 is a major regulator of OPC response to injury during early postnatal development and in the adult brain.

We extensively explored the involvement of Rb—a direct downstream target of Cdk2—in the molecular pathways activated by hypoxia in white matter. Rb phosphorylation, particularly at Ser 807/811, has been identified as a major molecular checkpoint for cell cycle progression (Gardner et al., 2001). Phosphorylation of Rb causes dissociation of the Rb–E2F1 complex with subsequent release of the E2F1 transcription factor. Consistent with this mechanism, we found higher levels of Rb phosphorylation and of unbound E2F1 in white matter after hypoxia, indicating that Rb phosphorylation at Ser 807/811 promoted G_1/S transition in OPCs (Harbour et al., 1999).

p27 ^{Kip1} regulates posthypoxic oligodendrogenesis in white matter

We also noted a significant decrease in p27 ^{Kip1} expression after hypoxia, with a time course consistent with a role for this Cdk inhibitor in preventing oligodendrocyte maturation. Analysis of p27 $^{-/-}$ mice—in which lack of p27 ^{Kip1} exacerbates the effects of hypoxia on oligodendrocyte and white matter development—confirmed a role for this protein in oligodendrocyte maturation under hypoxic conditions. Furthermore, p27 ^{Kip1} overexpression promoted oligodendrogenesis in cultures obtained from hypoxic white matter or in white matter *in vivo*. In summary, our results demonstrate a functional role for p27 ^{Kip1} in promoting oligodendrocyte regeneration in pathologies associated with white matter deficit (Katchanov et al., 2001; Crockett et al., 2005; Shen et al., 2008). These findings are consistent with previous *in vitro* studies, as well as studies in transgenic mice that identified p27 ^{Kip1} as a main regulator of oligodendrocyte differentiation and maturation (Casaccia-Bonnefil et al., 1999; Ghiani et al., 1999; Chew et al., 2005). p27 ^{Kip1} has been shown to control the oxygen-dependent checkpoint in late G_1 of the cell cycle, when the Cdk2 pathway is most active (Graff et al., 2005). Our experimental paradigm of neonatal hypoxia demonstrates an inverse correlation between Cdk2 and p27 ^{Kip1} protein levels in white matter, during a period when the increase in OPC proliferation is maximal and oligodendrocyte maturation is delayed. Importantly, the effects of hypoxia on expression of these two proteins were reversed later on, during developmental recovery, indicating probable involvement of p27^{Kip1} in the late arrest of OPC proliferation and subsequent oligodendrocyte differentiation. Expression of Cdk2 and p27 ^{Kip1} proteins in white matter after long-term recovery from hypoxia supports this interpretation, and is consistent with the increased number of mature oligodendrocytes after long-term recovery in normoxia.

It has been established that regulation of p27 ^{Kip1} expression involves forkhead transcription factors, particularly FoxO3a (Miyamoto et al., 2007). Although a significant increase in phospho-FoxO was observed at 2 h after hypoxia in adult hippocampus (Zhan et al., 2010), we found the opposite effect on FoxO protein expressions in white matter. The developmental time course of FoxO1, FoxO3a, and FoxO4 expression after neonatal hypoxia paralleled that of p27 ^{Kip1}, with FoxO1 being mostly affected. This suggested that lower levels of FoxO proteins were responsible for the reduction of p27 ^{Kip1} expression observed after hypoxia, and regulation of these proteins may promote oligodendrocyte regeneration in white matter after DWMI. This hypothesis was confirmed by gain- and loss-of-function experiments. Overexpression of FoxO1 in white matter cells after hypoxia led to oligodendrocyte recovery. Conversely, silencing FoxO1 expression in normoxic cells significantly reduced oligodendrogenesis.

It is also known that p27 ^{Kip1} regulators (FoxO genes) are altered by posttranslational modification, including ubiquitination by Skp2 (Huang and Tindall, 2011). Here, we demonstrate that neonatal hypoxia upregulates Skp2 during the first week after the insult *in vivo*, concomitantly with a downregulation of p27 ^{Kip1} and FoxO proteins expression. Furthermore, we show that, in cells isolated from hypoxic white matter, transfection with Skp2 siRNA and subsequent upregulation of p27 ^{Kip1} expression promoted oligodendrogenesis. Thus, our results demonstrate that posttranscriptional degradation of p27 ^{Kip1} occurs via FoxO proteins—mainly FoxO1—and by Skp2-mediated ubiquitination.

Conclusion

Our understanding of the cellular dynamics and molecular mechanisms contributing to neonatal brain damage—including DWMI—is still very limited. The present study reveals that, in developing white matter, the primary effects of hypoxic insult are hypomyelination as well as Cdk2-dependent OPC proliferation and delayed oligodendrogenesis. We also demonstrate that FoxO1-mediated p27 ^{Kip1} regulation is responsible for promoting oligodendrogenesis after neonatal hypoxia. Therefore, FoxO1 and p27 ^{Kip1} represent attractive molecular targets for restoring timely oligodendrogenesis after neonatal brain injury.

Acknowledgments

This work was supported by National Institutes of Health Grants P01 NS062686 (V.G., T.L.H., F.V.), R01 NS045702 (V.G.), R01 NS056427 (V.G.), T32 HD046388 (V.G., B.J.), and K12 NS052159 and K08 NS073793 (J.S.), and Pioneer Award OD006850 (T.L.H.). D.H.R. is a Howard Hughes Medical Institute investigator. We thank Dr. Marla Luskin for providing the p27 ^{Kip1} retrovirus and Dr. Domenico Accili for proving pCMV(5) HA FoxO1 plasmid. We are particularly grateful to Dr. Marcin Gierdalski for statistical analysis of data, writing a program facilitating processing of confocal images, and critical comments on this manuscript. We also thank Drs. Judy Liu and Li-Jin Chew for discussion and critically reading this paper. We thank Dr. Li-Jin Chew for help in plasmid preparation and Mackenzie Catron-Walden for breeding CNP-EGFP mice.

References

Aguirre A, Gallo V. Postnatal neurogenesis and gliogenesis in the olfactory bulb from NG2-expressing progenitors of the subventricular zone. J Neurosci. 2004; 24:10530–10541. [PubMed: 15548668]

Aguirre A, Dupree JL, Mangin JM, Gallo V. A functional role for EGFR signaling in myelination and remyelination. Nat Neurosci. 2007; 10:990–1002. [PubMed: 17618276]

Armstrong RC, Le TQ, Frost EE, Borke RC, Vana AC. Absence of fibroblast growth factor 2 promotes oligodendroglial repopulation of demyelinated white matter. J Neurosci. 2002; 22:8574–8585. [PubMed: 12351731]

Back SA. Perinatal white matter injury: the changing spectrum of pathology and emerging insights into pathogenetic mechanisms. Ment Retard Dev Disabil Res Rev. 2006; 12:129–140. [PubMed: 16807910]

Back SA, Luo NL, Borenstein NS, Levine JM, Volpe JJ, Kinney HC. Late oligodendrocyte progenitors coincide with the developmental window of vulnerability for human perinatal white matter injury. J Neurosci. 2001; 21:1302–1312. [PubMed: 11160401]

Back SA, Han BH, Luo NL, Chricton CA, Xanthoudakis S, Tam J, Arvin KL, Holtzman DM. Selective vulnerability of late oligodendrocyte progenitors to hypoxia-ischemia. J Neurosci. 2002; 22:455– 463. [PubMed: 11784790]

Beijersbergen RL, Carlée L, Kerkhoven RM, Bernards R. Regulation of the retinoblastoma protein-related p107 by G_1 cyclin complexes. Genes Dev. 1995; 9:1340–1353. [PubMed: 7797074]

Belachew S, Chittajallu R, Aguirre AA, Yuan X, Kirby M, Anderson S, Gallo V. Postnatal NG2 proteoglycan-expressing progenitor cells are intrinsically multipotent and generate functional neurons. J Cell Biol. 2003; 161:169–186. [PubMed: 12682089]

Berthet C, Aleem E, Coppola V, Tessarollo L, Kaldis P. Cdk2 knockout mice are viable. Curr Biol. 2003; 13:1775–1785. [PubMed: 14561402]

Bi B, Salmaso N, Komitova M, Simonini MV, Silbereis J, Cheng E, Kim J, Luft S, Ment LR, Horvath TL, Schwartz ML, Vaccarino FM. Cortical GFAP positive cells generate neurons after perinatal hypoxic injury. J Neurosci. 2011; 31:9205–9221. [PubMed: 21697371]

Billiards SS, Haynes RL, Folkerth RD, Borenstein NS, Trachtenberg FL, Rowitch DH, Ligon KL, Volpe JJ, Kinney HC. Myelin abnormalities without oligodendrocyte loss in periventricular leukomalacia. Brain Pathol. 2008; 18:153–163. [PubMed: 18177464]

Buser JR, Maire J, Riddle A, Gong X, Nguyen T, Nelson K, Luo NL, Ren J, Struve J, Sherman LS, Miller SP, Chau V, Hendson G, Ballabh P, Grafe MR, Back SA. Arrested preoligodendrocyte maturation contributes to myelination failure in premature infants. Ann Neurol. 2012; 71:93–109. [PubMed: 22275256]

Caillava C, Vandenbosch R, Jablonska B, Deboux C, Spigoni G, Gallo V, Malgrange B, Baron-Van Evercooren A. Cdk2 loss accelerates precursor differentiation and remyelination in the adult central nervous system. J Cell Biol. 2011; 193:397–407. [PubMed: 21502361]

Casaccia-Bonnefil P, Tikoo R, Kiyokawa H, Friedrich V Jr, Chao MV, Koff A. Oligodendrocyte precursor differentiation is perturbed in the absence of the cyclin-dependent kinase inhibitor p27 ^{Kip1}. Genes Dev. 1997; 11:2335–2346. [PubMed: 9308962]

Casaccia-Bonnefil P, Hardy RJ, Teng KK, Levine JM, Koff A, Chao MV. Loss of p27 ^{Kip1} function results in increased proliferative capacity of oligodendrocyte progenitors but unaltered timing of differentiation. Development. 1999; 126:4027– 4037. [PubMed: 10457012]

Chew LJ, King WC, Kennedy A, Gallo V. Interferon-γ inhibits cell cycle exit in differentiating oligodendrocyte progenitor cells. Glia. 2005; 52:127–143. [PubMed: 15920731]

Crockett DP, Burshteyn M, Garcia C, Muggironi M, Casaccia-Bonnefil P. Number of oligodendrocyte progenitors recruited to the lesioned spinal cord is modulated by the levels of the cell cycle regulatory protein p27 $^{Kip-1}$. Glia. 2005; 49:301–308. [PubMed: 15472992]

Dehan E, Pagano M. Skp2, the FoxO1 hunter. Cancer Cell. 2005; 7:209–210. [PubMed: 15766658]

Durand B, Gao FB, Raff M. Accumulation of the cyclin-dependent kinase inhibitor p27/Kip1 and the timing of oligodendrocyte differentiation. EMBO J. 1997; 16:306–317. [PubMed: 9029151]

Fagel DM, Ganat Y, Cheng E, Silbereis J, Ohkubo Y, Ment LR, Vaccarino FM. Fgfr1 is required for cortical regeneration and repair after perinatal hypoxia. J Neurosci. 2009; 29:1202–1211. [PubMed: 19176828]

Fero ML, Rivkin M, Tasch M, Porter P, Carow CE, Firpo E, Polyak K, Tsai LH, Broudy V, Perlmutter RM, Kaushansky K, Roberts JM. A syndrome of multiorgan hyperplasia with features of gigantism, tumorigenesis, and female sterility in p27 ^{Kip1}-deficient mice. Cell. 1996; 85:733–744. [PubMed: 8646781]

Frost EE, Nielsen JA, Le TQ, Armstrong RC. PDGF and FGF2 regulate oligodendrocyte progenitor responses to demyelination. J Neurobiol. 2003; 54:457–472. [PubMed: 12532397]

Gardner LB, Li Q, Park MS, Flanagan WM, Semenza GL, Dang CV. Hypoxia inhibits G_1/S transition through regulation of p27 expression. J Biol Chem. 2001; 276:7919–7926. [PubMed: 11112789]

Ghiani CA, Gallo V. Inhibition of cyclin E-cyclin-dependent kinase 2 complex formation and activity is associated with cell cycle arrest and withdrawal in oligodendrocyte progenitor cells. J Neurosci. 2001; 21:1274–1282. [PubMed: 11160398]

Ghiani CA, Yuan X, Eisen AM, Knutson PL, DePinho RA, McBain CJ, Gallo V. Voltage-activated K + channels and membrane depolarization regulate accumulation of the cyclin-dependent kinase inhibitors p27 ^{Kip1} and p21 ^{CIP1} in glial progenitor cells. J Neurosci. 1999; 19:5380–5392. [PubMed: 10377348]

Graff P, Amellem O, Seim J, Stokke T, Pettersen EO. The role of p27 in controlling the oxygen-dependent checkpoint of mammalian cells in late G_1. Anticancer Res. 2005; 25:2259–2267. [PubMed: 16158973]

Hack M, Wilson-Costello D, Friedman H, Taylor GH, Schluchter M, Fanaroff AA. Neurodevelopment and predictors of outcomes of children with birth weights of less than 1000 g: 1992–1995. Arch Pediatr Adolesc Med. 2000; 154:725–731. [PubMed: 10891026]

Harbour JW, Luo RX, Dei Santi A, Postigo AA, Dean DC. Cdk phosphorylation triggers sequential intramolecular interactions that progressively block Rb functions as cells move through G_1. Cell. 1999; 98:859– 869. [PubMed: 10499802]

Huang H, Tindall DJ. Regulation of FOXO protein stability via ubiquitination and proteasome degradation. Biochim Biophys Acta. 2011; 1813:1961–1964. [PubMed: 21238503]

Jablonska B, Aguirre A, Vandenbosch R, Belachew S, Berthet C, Kaldis P, Gallo V. Cdk2 is critical for proliferation and self-renewal of neural progenitor cells in the adult subventricular zone. J Cell Biol. 2007; 179:1231–1245. [PubMed: 18086919]

Katchanov J, Harms C, Gertz K, Hauck L, Waeber C, Hirt L, Priller J, von Harsdorf R, Bruck W, Hortnagl H, Dirnagl U, Bhide PG, Endres M. Mild cerebral ischemia induces loss of cyclin-dependent kinase inhibitors and activation of cell cycle machinery before delayed neuronal cell death. J Neurosci. 2001; 21:5045–5053. [PubMed: 11438580]

Kinney HC, Back SA. Human oligodendroglial development: relationship to periventricular leukomalacia. Semin Pediatr Neurol. 1998; 5:180–189. [PubMed: 9777676]

Krtolica A, Krucher NA, Ludlow JW. Hypoxia-induced pRB hypophosphorylation results from downregulation of CDK and upregulation of PP1 activities. Oncogene. 1998; 17:2295–2304. [PubMed: 9811460]

Lachapelle F, Avellana-Adalid V, Nait-Oumesmar B, Baron-Van Evercooren A. Fibroblast growth factor-2 (FGF-2) and platelet-derived growth factor AB (PDGF AB) promote adult SVZ-derived oligodendrogenesis in vivo. Mol Cell Neurosci. 2002; 20:390–403. [PubMed: 12139917]

Luskin MB. Restricted proliferation and migration of postnatally generated neurons derived from the forebrain subventricular zone. Neuron. 1993; 11:173–189. [PubMed: 8338665]

Menn B, Garcia-Verdugo JM, Yaschine C, Gonzalez-Perez O, Rowitch D, Alvarez-Buylla A. Origin of oligodendrocytes in the subventricular zone of the adult brain. J Neurosci. 2006; 26:7907–7918. [PubMed: 16870736]

Ment LR, Constable RT. Injury and recovery in the developing brain: evidence from functional MRI studies of prematurely born children. Nat Clin Pract Neurol. 2007; 3:558–571. [PubMed: 17914344]

Ment LR, Schwartz M, Makuch RW, Stewart WB. Association of chronic sublethal hypoxia with ventriculomegaly in the developing rat brain. Brain Res Dev Brain Res. 1998; 111:197–203.

Ment LR, Schneider KC, Ainley MA, Allan WC. Adaptive mechanisms of developing brain. The neuroradiologic assessment of the preterm infant. Clin Perinatol. 2000; 27:303–323. [PubMed: 10863652]

Ment LR, Vohr B, Allan W, Katz KH, Schneider KC, Westerveld M, Duncan CC, Makuch RW. Change in cognitive function over time in very low-birth-weight infants. JAMA. 2003; 289:705–711. [PubMed: 12585948]

Miyamoto K, Araki KY, Naka K, Arai F, Takubo K, Yamazaki S, Matsuoka S, Miyamoto T, Ito K, Ohmura M, Chen C, Hosokawa K, Nakauchi H, Nakayama K, Nakayama KI, Harada M, Motoyama N, Suda T, Hirao A. Foxo3a is essential for maintenance of the hematopoietic stem cell pool. Cell Stem Cell. 2007; 1:101–112. [PubMed: 18371339]

Myatt SS, Lam EW. The emerging roles of forkhead box (Fox) proteins in cancer. Nat Rev Cancer. 2007; 7:847–859. [PubMed: 17943136]

Nait-Oumesmar B, Picard-Riéra N, Kerninon C, Baron-Van Evercooren A. The role of SVZ-derived neural precursors in demyelinating diseases: from animal models to multiple sclerosis. J Neurol Sci. 2008; 265:26–31. [PubMed: 17961598]

Ness JK, Romanko MJ, Rothstein RP, Wood TL, Levison SW. Perinatal hypoxia-ischemia induces apoptotic and excitotoxic death of periventricular white matter oligodendrocyte progenitors. Dev Neurosci. 2001; 23:203–208. [PubMed: 11598321]

Nguyen L, Borgs L, Vandenbosch R, Mangin JM, Beukelaers P, Moonen G, Gallo V, Malgrange B, Belachew S. The yin and yang of cell cycle progression and differentiation in the oligodendroglial lineage. Ment Retard Dev Disabil Res Rev. 2006; 12:85–96. [PubMed: 16807909]

Raymond M, Li P, Mangin JM, Huntsman M, Gallo V. Chronic perinatal hypoxia reduces glutamate-aspartate transporter function in astrocytes through the Janus kinase/signal transducer and activator of transcription pathway. J Neurosci. 2011; 31:17864–17871. [PubMed: 22159101]

Sanai N, Tramontin AD, Quiñones-Hinojosa A, Barbaro NM, Gupta N, Kunwar S, Lawton MT, McDermott MW, Parsa AT, Manuel-García Verdugo J, Berger MS, Alvarez-Buylla A. Unique

astrocyte ribbon in adult human brain contains neural stem cells but lacks chain migration. Nature. 2004; 427:740–744. [PubMed: 14973487]

Scafidi J, Fagel DM, Ment LR, Vaccarino FM. Modeling premature brain injury and recovery. Int J Dev Neurosci. 2009; 27:863– 871. [PubMed: 19482072]

Shen A, Liu Y, Zhao J, Qin J, Shi S, Chen M, Gao S, Xiao F, Lu Q, Cheng C. Temporal-spatial expressions of p27 ^{kip1} and its phosphorylation on serine-10 after acute spinal cord injury in adult rat: implications for post-traumatic glial proliferation. Neurochem Int. 2008; 52:1266–1275. [PubMed: 18319192]

Tikoo R, Osterhout DJ, Casaccia-Bonnefil P, Seth P, Koff A, Chao MV. Ectopic expression of p27 ^{Kip1} in oligodendrocyte progenitor cells results in cell-cycle growth arrest. J Neurobiol. 1998; 36:431–440. [PubMed: 9733077]

Volpe JJ. Perinatal brain injury: from pathogenesis to neuroprotection. Ment Retard Dev Disabil Res Rev. 2001; 7:56–64. [PubMed: 11241883]

Wood NS, Marlow N, Costeloe K, Gibson AT, Wilkinson AR. Neurologic and developmental disability after extremely preterm birth. EPICure Study Group. N Engl J Med. 2000; 343:378–384. [PubMed: 10933736]

Yang JY, Hung MC. A new fork for clinical application: targeting forkhead transcription factors in cancer. Clin Cancer Res. 2009; 15:752–757. [PubMed: 19188143]

Zhan L, Wang T, Li W, Xu ZC, Sun W, Xu E. Activation of Akt/FoxO signaling pathway contributes to induction of neuroprotection against transient global cerebral ischemia by hypoxic pre-conditioning in adult rats. J Neurochem. 2010; 114:897–908. [PubMed: 20492357]

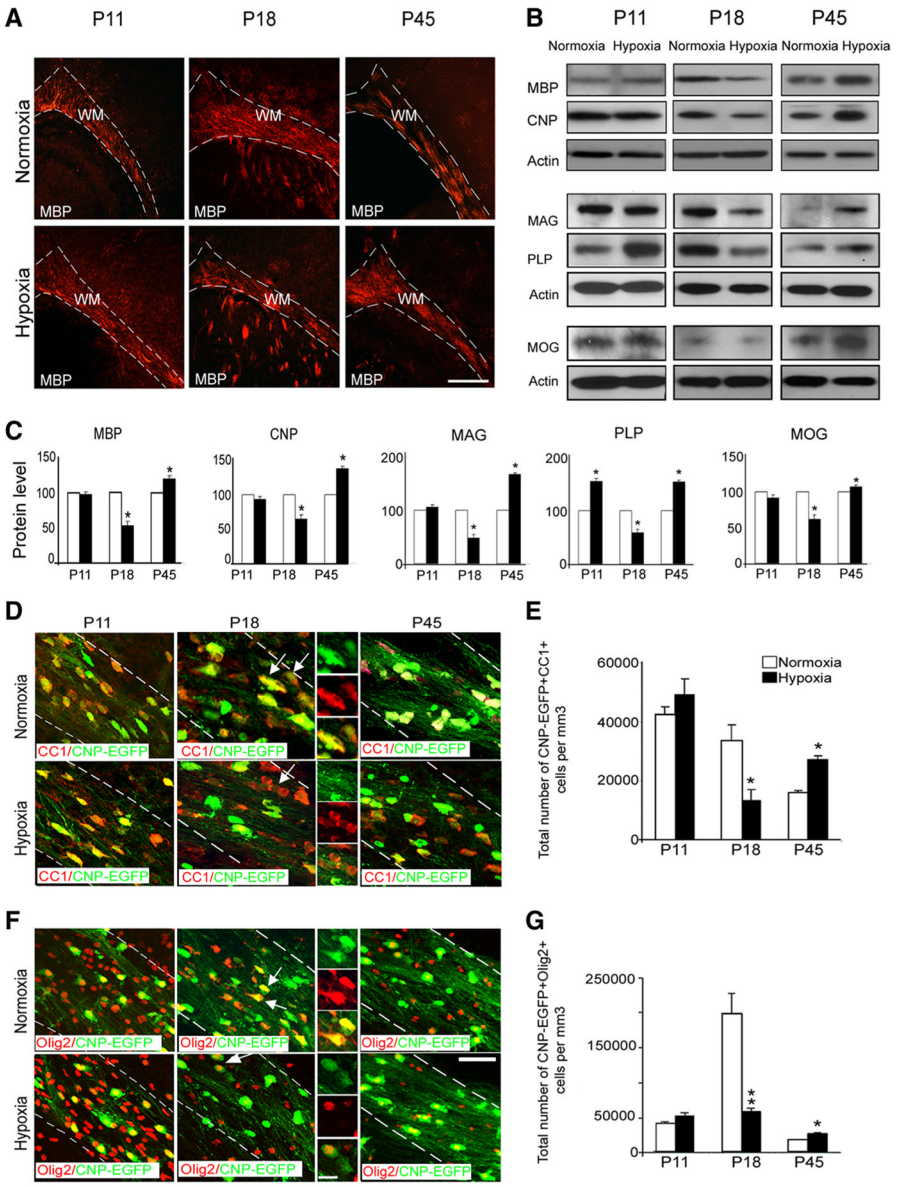

Figure 1.

Hypoxia causes hypomyelination during white matter development. ***A***, Confocal images of white matter from normoxic and hypoxic brains at P11, P18, and P45 immunostained with anti-MBP antibody. The dotted lines bound white matter. WM, White matter. Scale bar, 100 μm (n =4 brains for each condition). ***B***, Western blot analysis of white matter dissected from hypoxic and normoxic brains at P11, P18, and P45 demonstrates developmental expression of MBP, CNP, MAG, PLP, and MOG; actin was used as a loading control. ***C***, Graphs represent transient changes in expressions of above proteins indicating a reduction in their level at P18, followed by an increase at P45 (n = 4 brains for each condition and for each antibody; *p <0.05, t test). Confocal, tricolored images from normoxic and hypoxic white matter at P11, P18, and P45. CNP-EGFP $^{+}$cells are stained with anti-CC1 (***D***) and anti-Olig2 (***F***) antibodies. The dotted lines bound white matter. The insets magnify cells pointed by white arrows. Scale bar, 30 μm. Graphs represent total number of CNP-EGFP $^{+}$cells expressing CC1 (***E***) and Olig2 (***G***) in normoxic and hypoxic white matter at P11, P18, and

P45. Hypoxia causes a significant reduction of CNP-EGFP $^{+}$CC1 $^{+}$ and CNP-EGFP $^{+}$Olig2 $^{+}$ cells at P18; however, a significant increase of oligodendrocytes is seen at P45. At P11, there was no difference in total number of oligodendrocytes in white matter after hypoxia (n = 4 brains for each condition, and for each antibody; *$p < 0.05$, **$p < 0.02$, t test). Error bars indicate SEM.

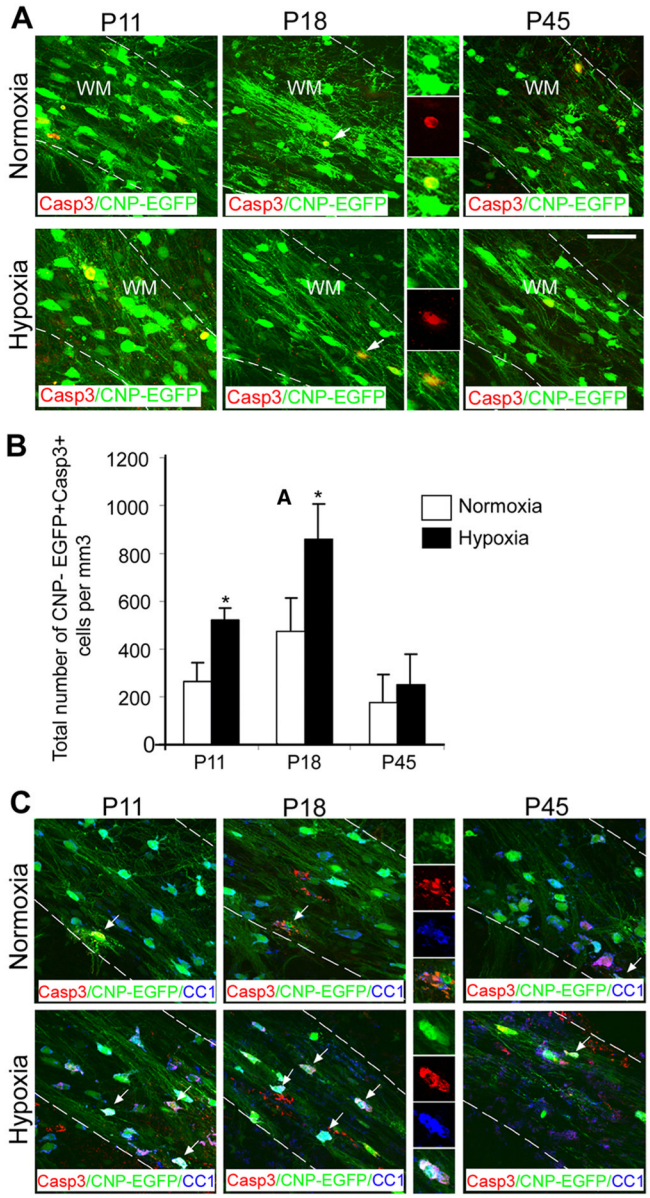

Figure 2.

Hypoxia increases apoptosis of oligodendrocytes. ***A***, Confocal images from normoxic and hypoxic white matter. CNP-EGFP $^{+}$cells were doubled-stained with anti-Caspase 3 antibody. The dotted lines bound white matter. The insets magnify cells pointed by white arrows. WM, White matter. Scale bar, 50 μm ($n = 4$ brains for each condition). ***B***, Increased apoptosis of CNP-EGFP $^{+}$cells in white matter was observed at P11 and P18 ($n = 4$ brains for each condition; *$p < 0.05$, t test). ***C***, Confocal images from normoxic and hypoxic white matter. CNP-EGFP $^{+}$cells were triple-stained with anti-Caspase 3 and anti-CC1 antibodies. The dotted lines bound white matter. The insets magnify cells pointed by white arrows. WM, White matter. Scale bar, 50 μm. Error bars indicate SEM.

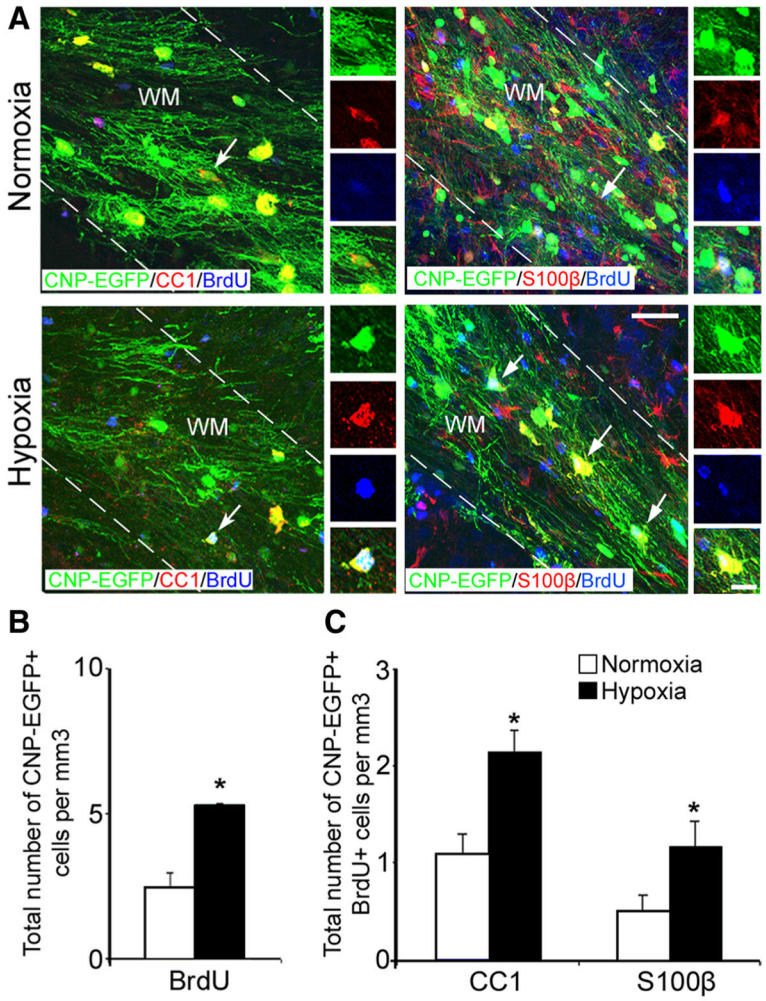

Figure 3.

Oligodendrocytes seen at P45 were generated immediately after hypoxia. ***A***, Confocal images from normoxic and hypoxic white matter at P45. CNP-EGFP $^{+}$BrdU $^{+}$cells are colabeled with anti-CC1 and anti-S100β antibodies. The dotted lines bound white matter. The insets magnify cells pointed by white arrows. WM, White matter. Scale bar, 50 μm. The graphs represent total number of proliferating CNP-EGFP $^{+}$ cells expressing BrdU (***B***), and CNP-EGFP $^{+}$BrdU $^{+}$CC1 $^{+}$ and CNP-EGFP $^{+}$BrdU $^{+}$S100β^{+}cells at P45 (***C***) (n = 4 brains for each condition and for each antibody; *$p < 0.05$, t test). Error bars indicate SEM.

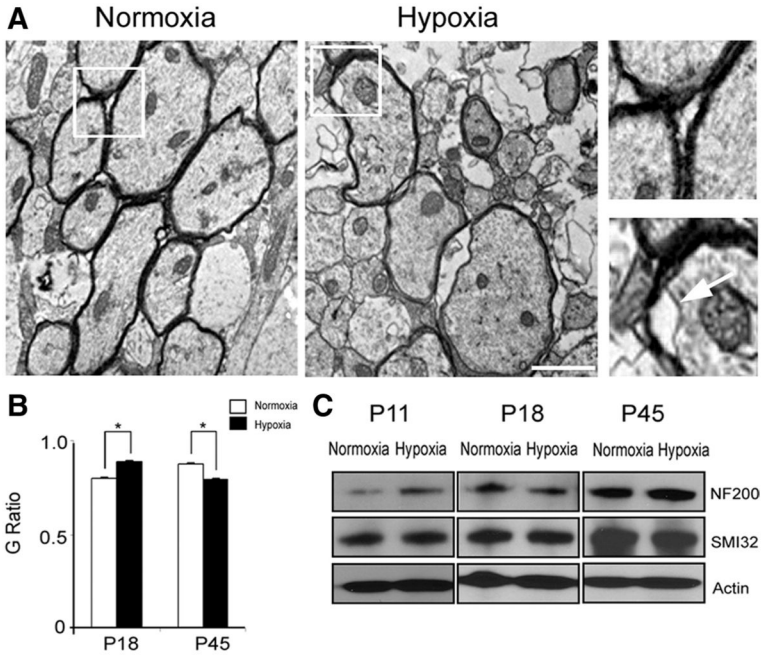

Figure 4.

Cellular recovery in oligodendrocytes does not correlate with proper axonal myelination. ***A***, Ultrastructure of myelinated and unmyelinated axons in the corpus callosum region after normoxia and hypoxia at P45. Scale bar, 1 μm. Higher magnification of images demonstrate proper axonal myelination (left panel, normoxia) and loosely wrapped, delaminated myelin (right panel, hypoxia). The white arrow points to loosely wrapped myelin. ***B***, Graph represents significant changes in *G* ratios after hypoxia compared with normoxia at P18 and P45 ($n = 3$ brains; total number of axons analyzed ranged between 38 and 49 for P18, and 32 and 56 for P45; $*p < 0.04$). ***C***, Western blot analysis from normoxic and hypoxic white matter demonstrates no changes in neurofilament protein expression (NF200, total, and SMI 32, nonphosphorylated) at P18 and P45. Hypoxia upregulates the expression of NF200 at P11 ($n = 3$ brains for each condition and each marker; $*p < 0.05$, *t* test). Error bars indicate SEM.

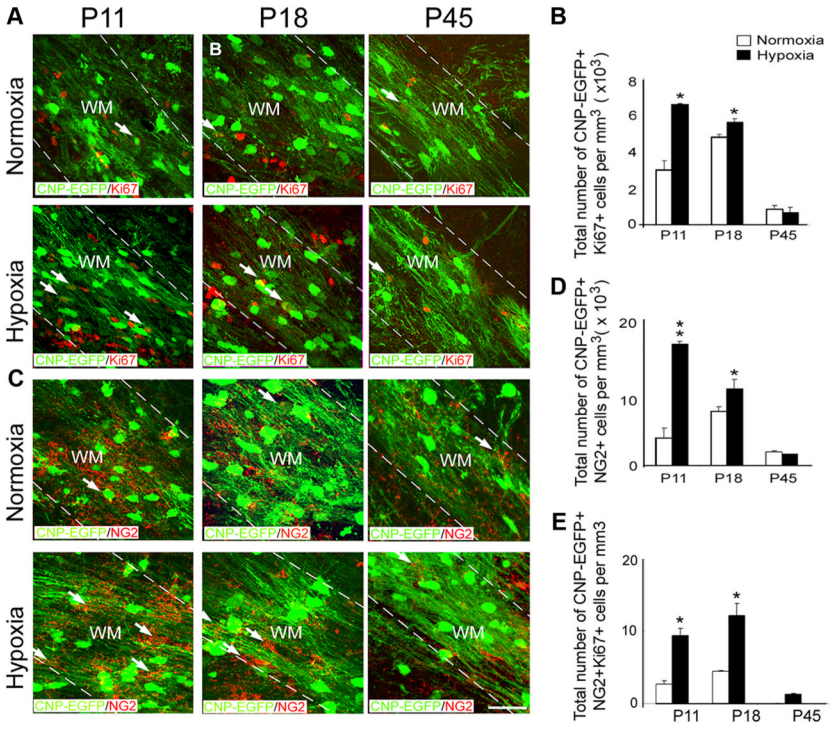

Figure 5.

Enhanced cell proliferation in white matter during the first week after hypoxia. Confocal images of white matter obtained from normoxic and hypoxic brains at P11, P18, and P45. CNP-EGFP $^{+}$cells were stained with anti-Ki67 (***A***) and anti-NG2 (***C***) antibodies. The white arrows point to double-labeled cells. The dotted lines bound white matter. WM, White matter. Scale bar, 50 μm. The graphs represent total numbers of CNP-EGFP $^{+}$Ki67 $^{+}$(***B***), CNP-EGFP $^{+}$NG2 $^{+}$(***D***), and CNP-EGFP $^{+}$NG2 $^{+}$Ki67 $^{+}$(***E***) cells. These cell populations were upregulated at P11 and P18 after hypoxia. No differences between hypoxia and normoxia were observed at P45 ($n = 4$ brains for each condition, and for each antibody; *$p <$ 0.05, **$p < 0.02$, t test). Error bars indicate SEM.

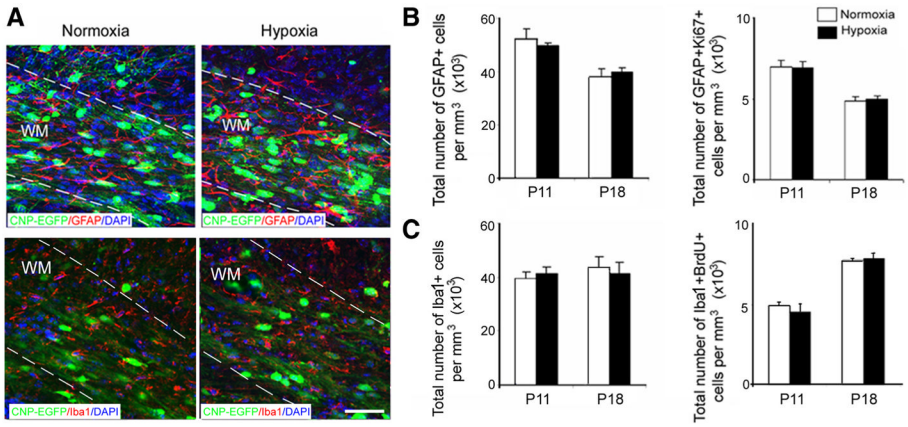

Figure 6.

Hypoxia does not affect astrocyte and microglia in white matter. ***A***, Confocal images from normoxic and hypoxic white matter at P18 demonstrating astrocytes labeled with GFAP and microglia labeled with Iba1. The dotted lines bound white matter. WM, White matter. Scale bar, 100 μm. The graphs present total number of GFAP $^{+}$and GFAP $^{+}$Ki67 $^{+}$(***B***), Iba1 and Iba1 $^{+}$BrdU $^{+}$ (***C***) at P11 and P18. No difference in total number of astrocytes and microglial cells, and their proliferation were detected in white matter immediately and 1 week after hypoxia (n = 4 brains for each condition and for each antibody). Error bars indicate SEM.

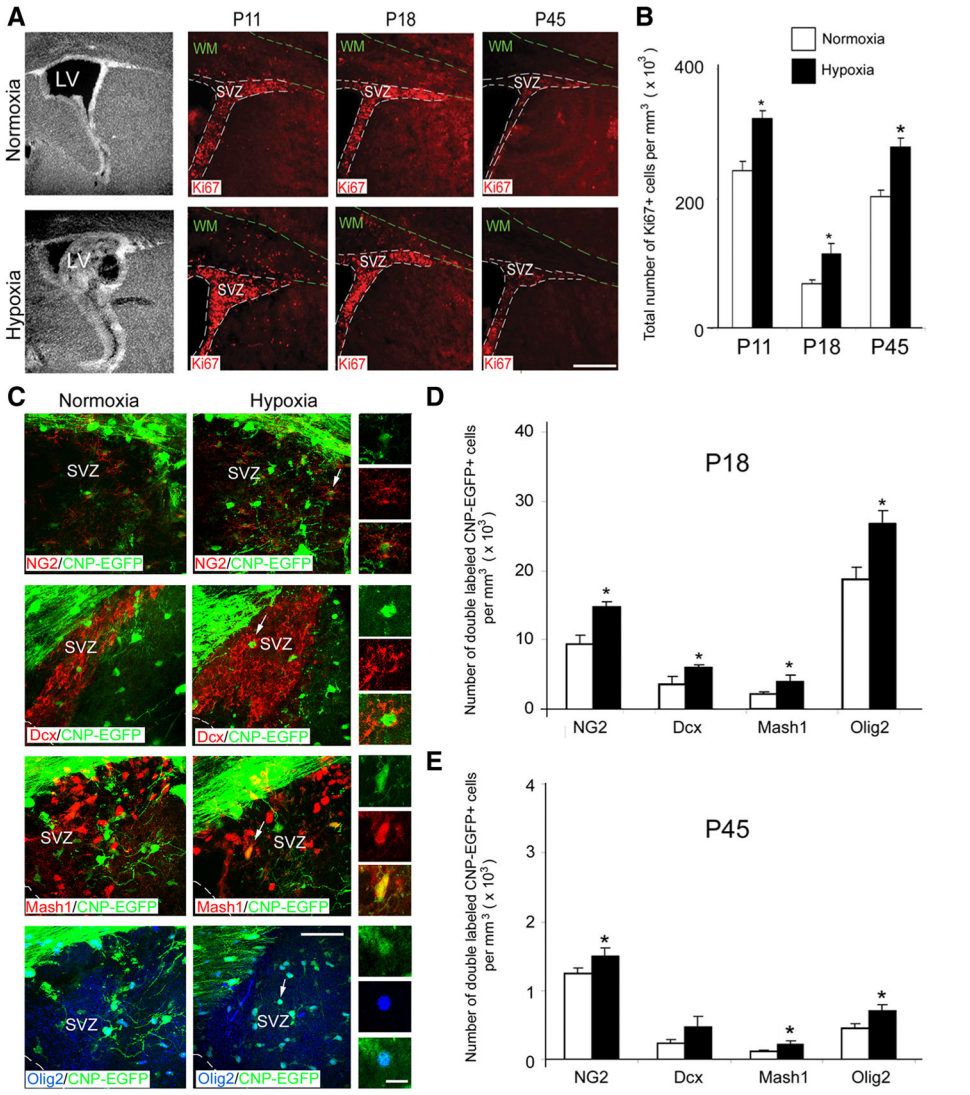

Figure 7.

Enhanced cell proliferation in hypoxic SVZ. ***A***, Enlargement of the lateral ventricles was observed at P18 after hypoxia, compared with normoxia. Confocal images show SVZ from normoxic and hypoxic brains at P11, P18, and P45 viewed at 10× magnification. Sections were stained with anti-Ki67 antibody for cell proliferation. After hypoxia, an expansion of the SVZ was observed at P11 and P18. The dotted lines bound the SVZ. WM, White matter. Scale bar, 100 μm ($n = 4$ brains for each condition). ***B***, Graph represents the total number of Ki67 $^{+}$cells in the SVZ at P11, P18, and P45. A significant increase in Ki67 $^{+}$cells was observed in the SVZ during development ($n = 4$ brains for each condition; $^{*}p < 0.05$, *t* test). ***C***, Confocal images of double-labeled cells from the SVZ at P18. CNP-EGFP $^{+}$cells labeled with anti-NG2, anti-Dcx, anti-Mash1, and anti-Olig2 antibodies. The insets magnify cells pointed by white arrows. Scale bar, 50μm. ***D***, Significantly more CNP-EGFP $^{+}$cells expressing NG2, Dcx, Mash1, and Olig2 were found at P18 in hypoxic versus normoxic SVZ ($n = 4$ brains for each condition, and for each antibody; $^{*}p < 0.05$, *t* test). ***E***, The SVZ progenitor cell response was still evident at P45, as demonstrated by an increase in the total number of NG2 $^{+}$, Mash1 $^{+}$, and Olig2 $^{+}$cells at this age ($n = 4$ brains for each condition, and for each antibody; $^{*}p < 0.05$, *t* test). Error bars indicate SEM.

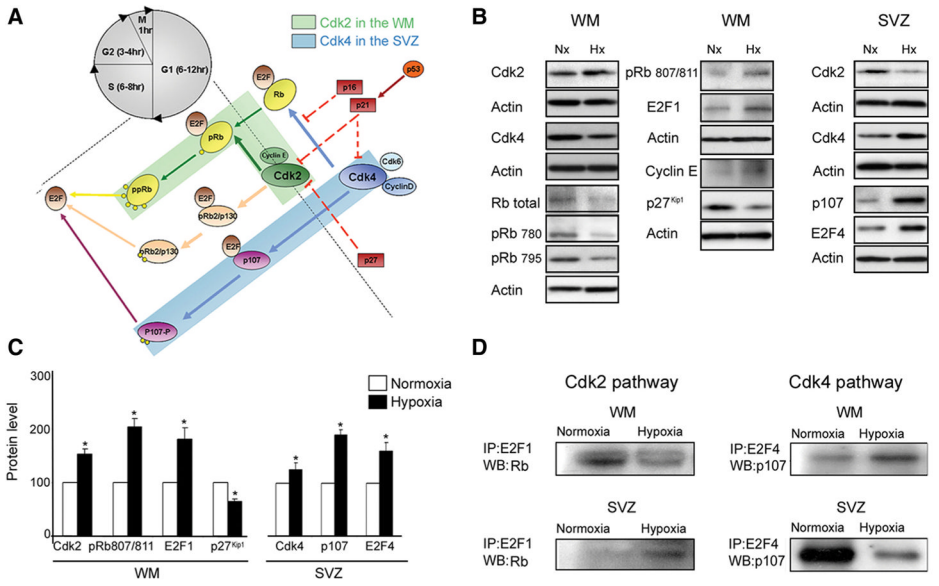

Figure 8.

Distinct pathways responsible for cell proliferation in white matter and SVZ after hypoxia. Cdk2 and Cdk4 are activated by hypoxia in white matter and SVZ, respectively. ***A***, Schematic drawing of the network of cell cycle proteins involved in proliferation in white matter and SVZ. ***B***, Western blot analysis of white matter and SVZ tissue dissected from P18 normoxic and hypoxic mice. Expression of Cdk2 and Cdk4, cyclin E, total Rb, pRb(Ser780), pRb(Ser795), pRb(Ser807/811), p107, E2F1, E2F4, and inhibitor, p27 ^{Kip1}, was analyzed. ***C***, Graphs represent an elevated expression of Cdk2, pRb807/811, E2F1, and reduced p27 ^{Kip1} in white matter after hypoxia. Higher levels of Cdk4, p107, and E2F4 were found in SVZ after hypoxia, compared with normoxia. Western blot analysis was performed on four independent WM and SVZ samples for each condition (*$p < 0.05$, *t* test). Actin was used as a loading control. ***D***, Immunoprecipitation assays performed on white matter and SVZ from normoxic and hypoxic P18 tissue. Rb–E2F1 and p107–E2F4 complexes were immunoprecipitated with anti-E2F1, and anti-E2F4 antibodies, respectively, and probed on Western blot with anti-Rb and anti-p107 antibodies. At P18, Rb expression was lower in hypoxic compared with normoxic white matter, while lower p107 expression was observed in hypoxic SVZ. Analysis was repeated on four independent WM and SVZ specimens for each condition. Western blot results are shown from a representative experiment. Error bars indicate SEM.

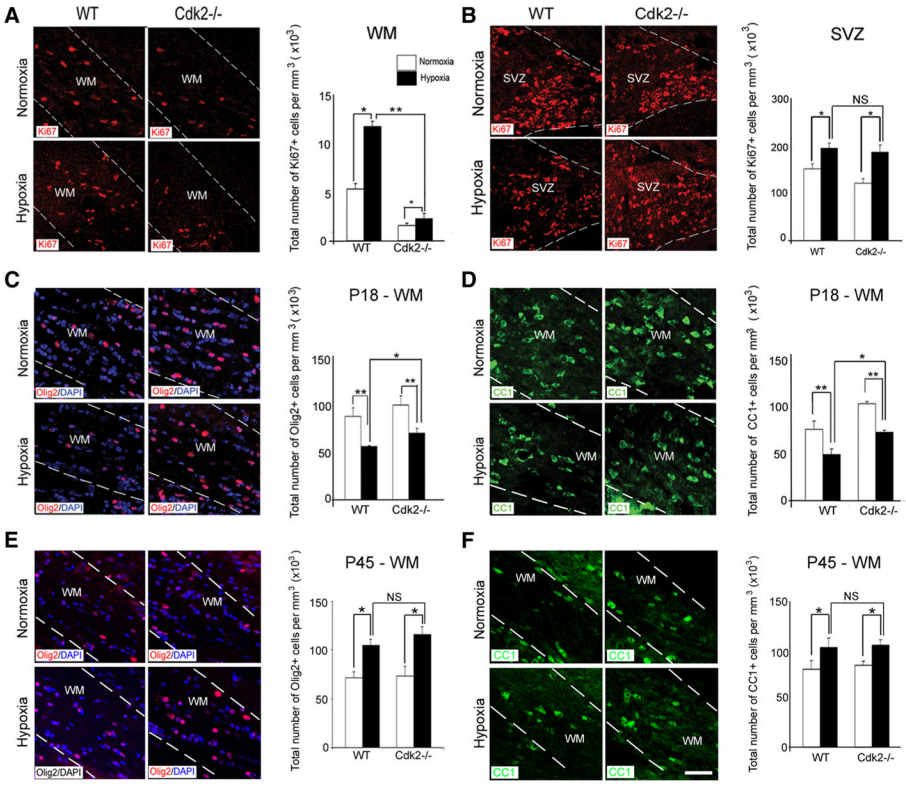

Figure 9.

Cdk2 is essential for oligodendrocyte development after hypoxia. Confocal images of white matter (***A***) and SVZ (***B***) from wild-type and Cdk2 $^{-/-}$mice after normoxia and hypoxia at P18. Proliferating cells were labeled with anti-Ki67 antibody. In Cdk2 $^{-/-}$mice, hypoxia caused a modest elevation in proliferation in white matter. A significant proliferative response was also sustained in the SVZ. The dotted lines bound white matter and SVZ. WM, White matter. Scale bar, 30 μm ($n = 4$ brains for each condition; *$p < 0.05$, **$p < 0.02$, two-way ANOVA). Confocal images of immunostaining with Olig2 and CC1 after normoxia and hypoxia at P18 in Cdk2 $^{-/-}$mice and their littermates at P18 and P45. Oligodendrocytes were labeled with Olig2 (***C***, ***E***) and CC1 (***D***, ***F***) markers. In wild-type and Cdk2 $^{-/-}$white matter, hypoxia reduced oligodendrocyte differentiation at P18, compared with normoxia, followed by a recovery at P45 ($n = 4$ brains for each condition, and for each antibody; *$p < 0.05$, **$p < 0.02$, two-way ANOVA). Error bars indicate SEM.

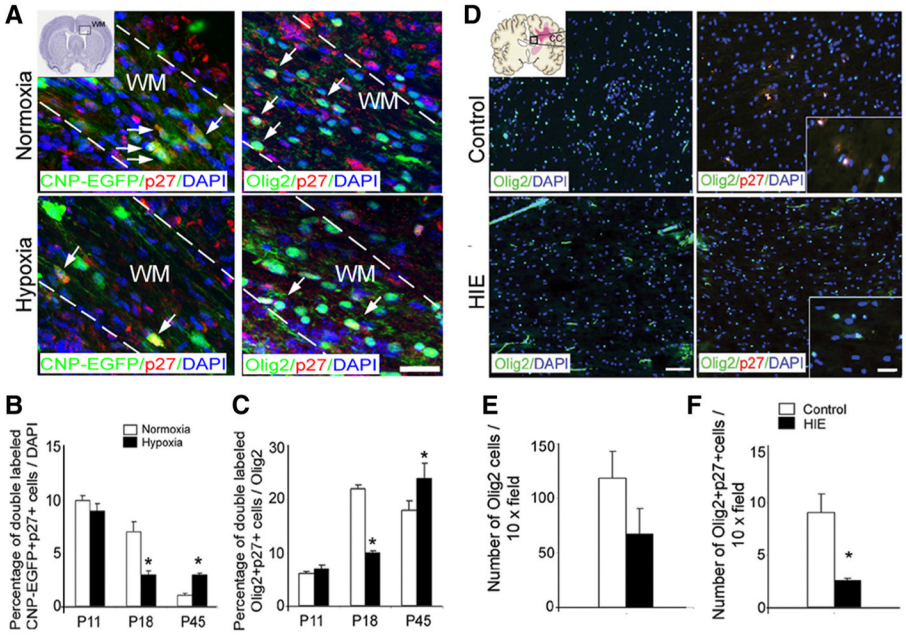

Figure 10.

Downregulation of p27 ^{Kip1} expression after hypoxia in mouse and human neonatal white matter. ***A***, Confocal images of white matter from normoxic and hypoxic brains at P18. White matter tissue was immunostained with anti-p27 ^{Kip1} and anti-Olig2 antibodies. The dotted lines bound white matter. WM, White matter. The white arrows point to cells expressing p27 ^{Kip1}. Scale bar, 100 μm. The graphs represent a reduction in the percentage of CNP-EGFP $^{+}$p27 $^{Kip1+}$(***B***) and CNP-EGFP $^{+}$Olig2 $^{+}$p27 $^{Kip1+}$(***C***) cells in white matter after hypoxia at P18, and a significant elevation in the percentage of these cells at P45 ($n = 4$ brains for each condition and for each antibody; $^{*}p < 0.05$). ***D***, Confocal images from human tissue from control and HIE newborns. Cells were stained with anti-Olig2 and anti-p27 ^{Kip1} Abs. The insets show a magnification of oligodendrocytes expressing p27 ^{Kip1}. Scale bars: Olig2 staining, 100 μm; Olig2/p27 staining, 100 μm. cc, Corpus callosum. The graphs represent lower number of Olig2 $^{+}$(***E***) and Olig2 $^{+}$p27 $^{Kip1+}$(***F***) cells in HIE patients compared with control in corpus callosum ($n = 3$ brains for each condition and for each antibody; $^{*}p < 0.02$). Error bars indicate SEM.

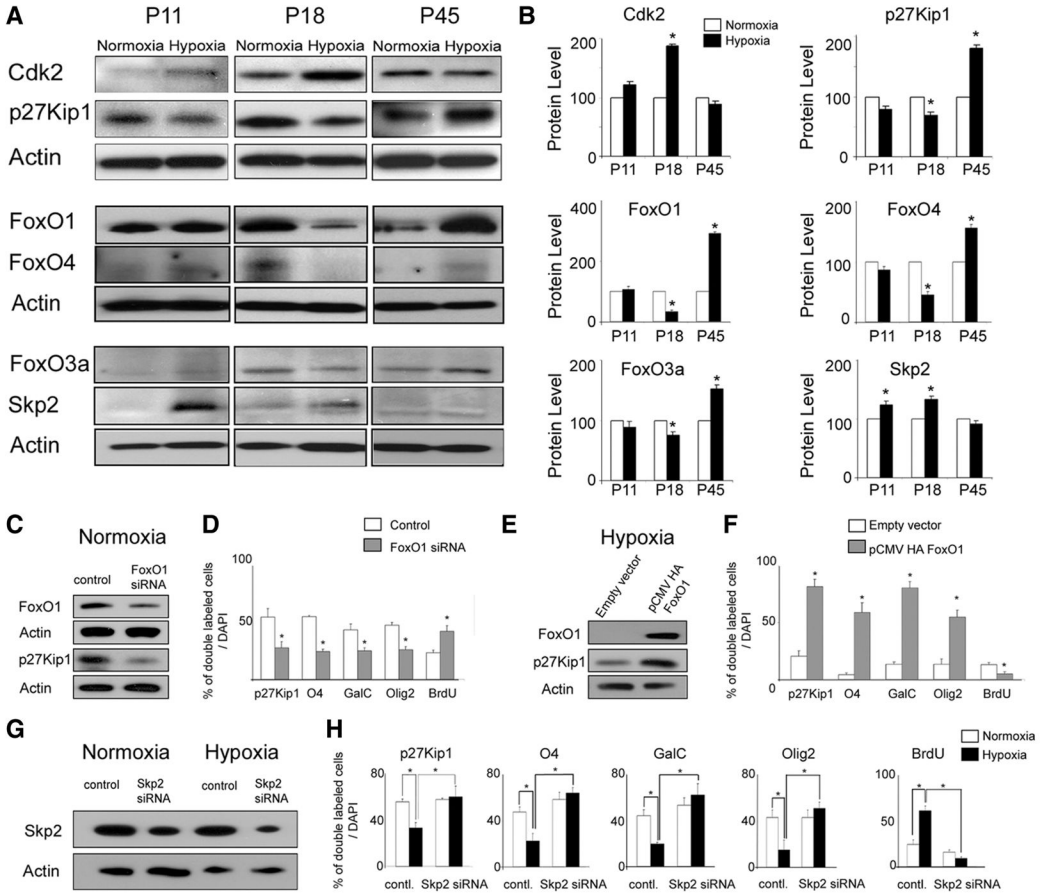

Figure 11.

FoxO1-dependent p27 ^{Kip1} expression in white matter OPCs after hypoxia. ***A***, Western blot analysis of Cdk2, p27 ^{Kip1}, FoxO1, FoxO4, FoxO3a, and Skp2 expression was performed in normoxic and hypoxic tissue at P11, P18, and P45. ***B***, Graphs show expression levels of Cdk2, p27 ^{Kip1}, FoxO1, FoxO4, FoxO3a, and Skp2 proteins quantified by Western blot. After hypoxia, Cdk2 and Skp2 levels were increased in white matter at P11 and P18. Conversely, p27 ^{Kip1}, FoxO1, FoxO3a, and FoxO4 levels were decreased by hypoxia at P18, but were elevated at P45. Actin was used as a loading control ($n = 4$ for normoxia and hypoxia, respectively; $^{*}p < 0.05$). ***C***, ***D***, FoxO1 loss of function in white matter cells in normoxic cultures. A reduction of 30–50% in FoxO1 and p27 ^{Kip1} levels was obtained after siRNA transfection. The graph shows the percentage of oligodendrocytes after FoxO1 siRNA and scrambled control transfection. In normoxic cultures, transfection with FoxO1 reduced the percentage of double-labeled EGFP $^{+}$ cells expressing p27 ^{Kip1}, O4, GalC, and Olig2, compared with cells transfected with scrambled control. However, the percentage of BrdU-proliferating cells was significantly elevated ($n = 4$ brains for each condition and for each antibody; $^{*}p < 0.05$). ***E***, ***F***, FoxO1 gain of function in white matter cells after hypoxia. Western blot analysis demonstrates a fivefold increase in FoxO1 expression levels after transfection with pCMV5 HA FoxO1 plasmid, compared with empty vector transfection. In differentiation assays, FoxO1 overexpression caused an increase in the percentage of EGFP $^{+}$cells expressing p27 ^{Kip1}, O4, GalC, and Olig2, and a reduction in proliferating cells, compared with cells transfected with empty vector ($n = 4$ brains for each condition and for each antibody; $^{*}p < 0.05$). ***G***, ***H***, Skp2 loss of function in normoxic and hypoxic white matter cells. Western blot analysis demonstrates lower expression of Skp2 protein after Skp2

siRNA transfection in normoxic and hypoxic white matter cells, compared with transfection with scrambled control siRNA. In hypoxic cultures, transfection with Skp2 siRNA increased the percentage of double-labeled EGFP $^{+}$cells expressing p27 ^{Kip1}, O4, GalC, and Olig2 oligodendrocytes, compared with normoxic cultures ($n = 4$ brains for each condition and for each antibody; $*p < 0.05$). Error bars indicate SEM.

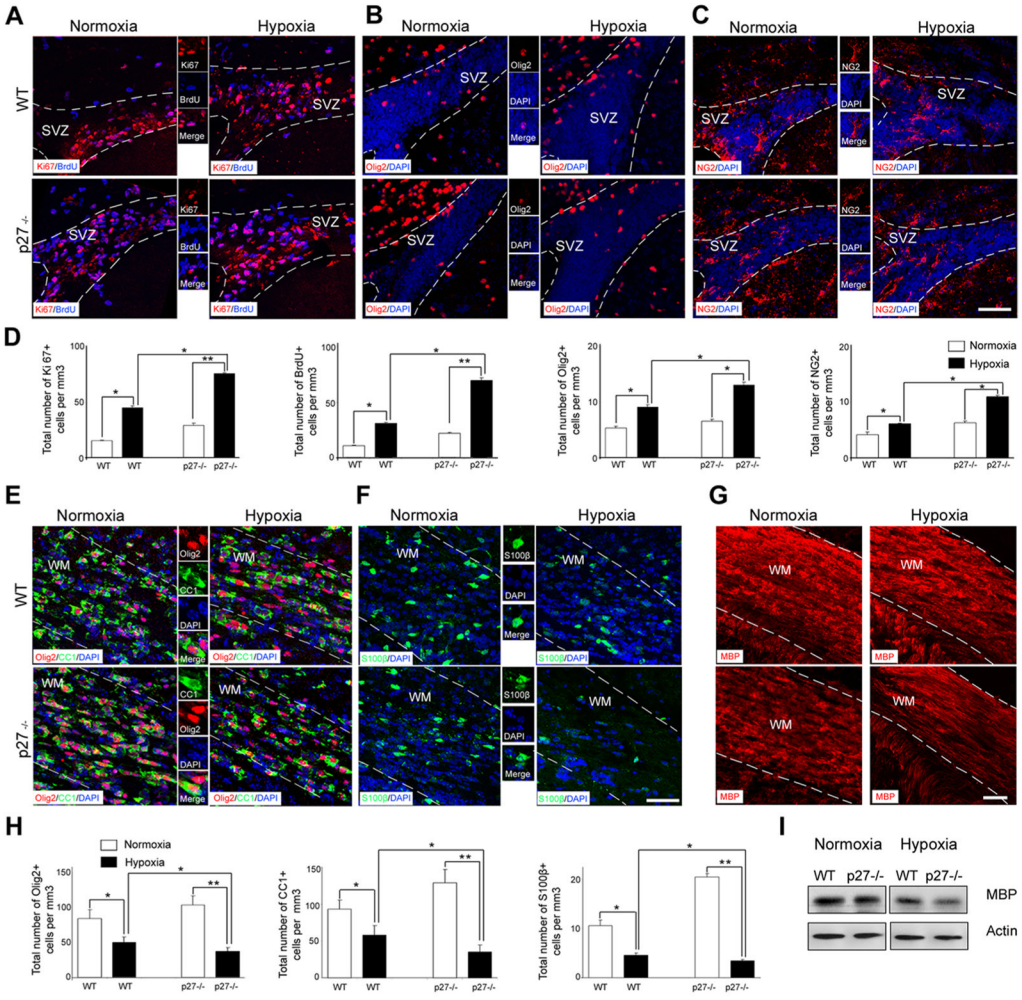

Figure 12.

The effects of hypoxia are exacerbated in white matter of p27 $^{-/-}$mice. Confocal images of SVZ from wild-type and p27 $^{-/-}$mice at P18 after normoxia and hypoxia. Proliferating cells were labeled with anti-Ki67 and anti-BrdU antibodies (***A***), and progenitor cells were labeled with anti-Olig2 (***B***) and anti-NG2 (***C***) antibodies. The dotted lines bound SVZ. Scale bar, 30 μm. ***D***, Graphs represent total number of Ki67 $^{+}$and BrdU $^{+}$cells in wild-type and p27 $^{-/-}$SVZ at P18 after hypoxia and normoxia ($n = 4$ brains for each condition, and for each antibody; *$p < 0.05$, **$p < 0.02$, two-way ANOVA). ***E–G***, Confocal images from hypoxic and normoxic white matter at P18. Sections were stained with anti-Olig2 and anti-CC1 (***E***), anti-S100β(***F***), and anti-MBP (***G***) antibodies. The dotted lines bound white matter (WM). Scale bar, 50 μm ($n = 3$ brains for each condition and for each antibody). ***H***, Graphs represent total number of Olig2 $^{+}$, CC1 $^{+}$, and S100β cells in white matter of wild-type and p27 $^{-/-}$mice after hypoxia and normoxia ($n = 3$ brains for each condition, and for each antibody; *$p < 0.05$, **$p < 0.02$, two-way ANOVA). ***I***, Western blots from wild-type and p27 $^{-/-}$tissue at P18 after hypoxia and normoxia. Lower MBP expression was found in p27 $^{-/-}$white matter after hypoxia. MBP expression was normalized against actin ($n = 3$ brains per condition). Error bars indicate SEM.

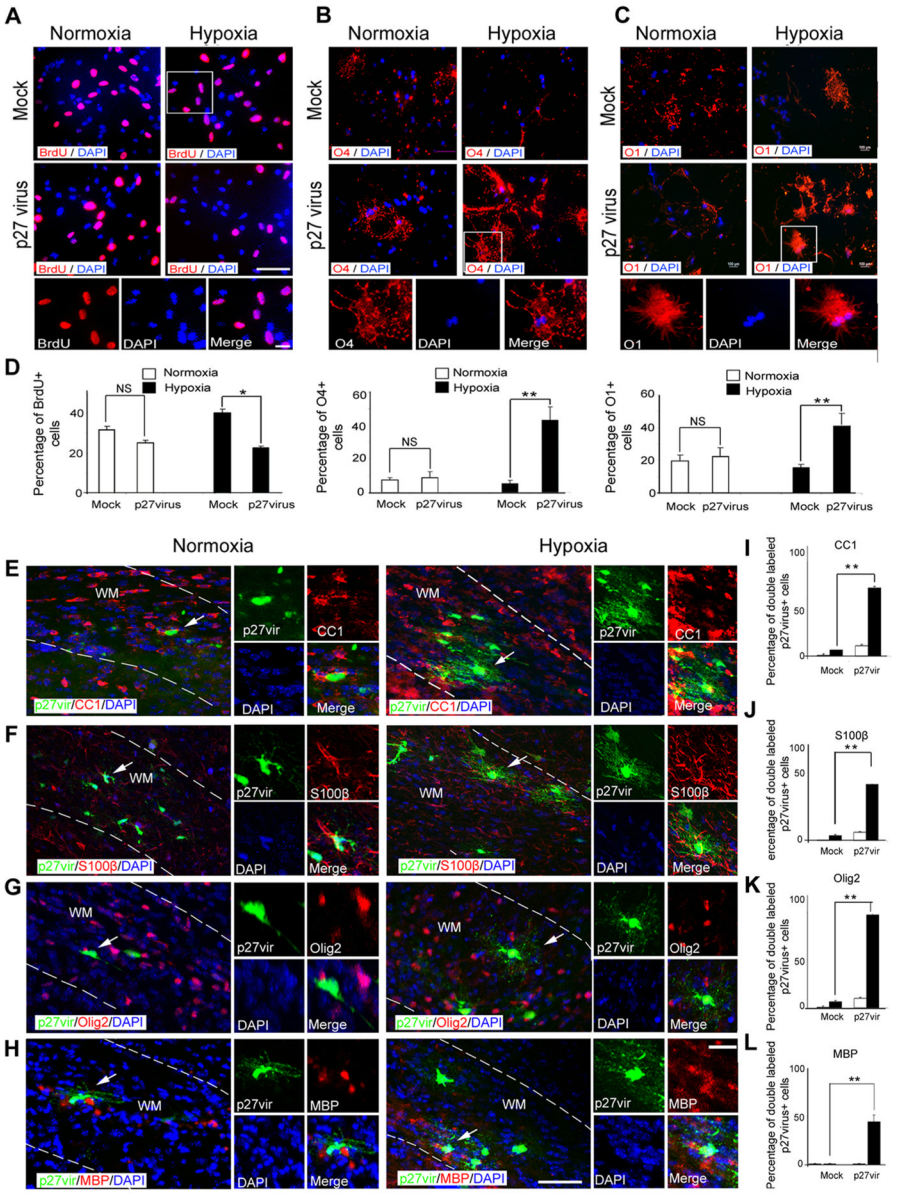

Figure 13.

p27 ^{Kip1} overexpression restores oligodendrocyte differentiation after hypoxia. ***A***, Cells from hypoxic and normoxic brains at P18 were transfected with p27 ^{Kip1} and mock retrovirus, and cultured 5 d in basal medium. For proliferation assays, cells were labeled with anti-BrdU antibody. The insets magnify cells in white boxes. Scale bar, 100 μm. For differential potential, cells were labeled with anti-O4 (***B***) and anti-O1 (***C***) antibodies. The insets magnify cells in white boxes. Scale bar, 100 μm. ***D***, Graphs represent the percentage of BrdU $^{+}$, O4 $^{+}$, and O1 $^{+}$cells compared with all DAPI cells. p27 ^{Kip1} overexpression increased the percentage of O4 $^{+}$and O1 $^{+}$cells after hypoxia compared with mock-virus transfection. In normoxic cells, p27 ^{Kip1} overexpression did not change percentage of oligodendrocytes ($n = 3$ brains for each condition; $^{*}p < 0.05$; $^{**}p < 0.02$; NS, nonsignificant, *t* test). p27 ^{Kip1} enhanced differentiation potential of oligodendrocytes after hypoxia *in vivo*. In white matter, cells labeled with p27 ^{Kip1} retrovirus were colabeled with CC1 (***E***), S100β (***F***), Olig2 (***G***), and MBP (***H***) markers after normoxia and hypoxia. The

insets magnify cells pointed by white arrows. WM, White matter. Scale bar, 50 μm. Graphs represent percentage of double-labeled p27virus $^{+}$cells stained with CC1 (***I***), S100β(***J***), Olig2 (***K***), and MBP (***L***) markers. After hypoxia, cells transfected with p27 ^{Kip1} retrovirus expressed Olig2, CC1, and S100β. In normoxia, p27 ^{Kip1} did not significantly change the number of mature oligodendrocytes compared with mock virus controls ($n = 4$ brains for each condition, and for each antibody; $^{*}p < 0.05$, two-way ANOVA). Error bars indicate SEM.

Table 1

Human developmental tissue

Case no.	Postnatal age	Gestational age at birth	Diagnosis	Area examined
Case 1	0 year, 56 d	37 weeks, 3 d	HIE	Corpus callosum
Case 2	0 year, 150 d	26 weeks, 0 d	HIE	Corpus callosum
Case 3	0 year, 58 d	37 weeks, 0 d	HIE	Corpus callosum
Case 4	0 year, 211 d	31 weeks, 0 d	Control	Corpus callosum
Case 5	0 year, 2 d	37 weeks, 3 d	Control	Corpus callosum
Case 6	0 year, 1 d	39 weeks, 0 d	Control	Corpus callosum